Norwegian University of
Science and Technology

Characterization of ZnS:Cr films for Intermediate Band Solar Cells

Tor Ingve Aamodt

Teacher Education with Master of Science
Submission date: June 2011
Supervisor: Ursula Gibson, IFY

Norwegian University of Science and Technology
Department of Physics

Abstract

In this thesis samples of ZnS:Cr thin films have been made through physical vapor deposition (PVD) with resistive heating and characterized by several methods. The thin films are of various thicknesses and contain different concentration of Cr. ZnS:Cr is a candidate to a bulk material for intermediate band solar cell, IBSC, and was therefore selected for this thesis. IBSC is a concept for solar cells with a much higher effiency than todays common solar cell.

The goal for the project was to put together the deposition system, make the samples, measure the thicknesses and concentrations and characterize them. Methods like X-Ray Diffraction (XRD), Auger electron spectroscopy (AES), profilometer, four point measurement, Hall-measurement and optical transmission measurements have been used to determine structure, concentrations, thicknesses, resistivity, number of carriers and transmission respectively.

The samples and the characterization performed with XRD, AES, profilometer, Hall-measurement and four point measurement were done at NTNU. The spectrum measurements were done at NTNU and the University in Vienna.

Samples with thicknesses in the range of 200 Å to 3340 Å have been investigated. Some were deposited in room temperature, some were annealed afterwards for 2 hours at 450^0C and some were deposited on substrates with a temperature of 300^0C. The thicknesses were measured with a contact profilometer. The theoretical concentration of the samples were in the range of 4% to 31%. There was impossible to measure samples with a lower concentration than 7%, even though these were made.

Transmission spectra were made in five overlapping specrophotometerss. Two were used in the visible region (UV-VIS), two in the near infra-red (NIR) region, and one Fourier Transform Infra-Red spectroscopy (FTIR) for the long wavelength region. The range was from 250 nm up to 25000 nm. No Cr^{2+} absorption lines were found. This can indicate a cluster form of the Cr and not a substitution of Cr^{2+} with Zn^{2+} ions. The band gap found from the transmission spectra were in the range of >4.5 eV to 2.95 eV. The high band gap imply insulating samples and inactive Cr states in cluster form.

No peaks from lattice configuration were found in the XRD spectrum. This

indicates an amorphous structure for both the samples deposited in room temperature, the annealed samples and the sample deposited on hot substrate. The lattice configuration of the sapphire substrate was found for 3 samples. This was the [300] reflection for sapphire at 68.2 degrees.

Four samples were investigated in AES. A 3340 Å 7% sample, a 800 Å <5% sample, a 370 Å 31% sample and a 830 Å >4% deposited on hot substrate. Less Cr than expected was found for the sample of 800 Å and 830 Å. However, all samples contained O and C. The sample deposited on hot substrate should contain 80 Å Cr theoretically, but no traces were found. The same applies for the 800 Å sample with less than 5%. Both charged badly which imply non-conductive samples. The 31% and the 7% sample did not show the same charging which implies conductivity. The samples showed a great amount of Cr, but did also contain O and C. However, from the Hall-measurement and four probe measurement none of the samples showed conductive properties. This emphasize the suspicion of incorporation of Cr clusters in inactive states making the samples insulating.

Preface

This thesis is written as a final work in my five years long education carrier at "Lektroutdanning i Realfag" (LUR), which is a masterprogram. The thesis is written during the spring 2011 and is a 30 points master thesis. My supervisor has been Ursula Gibson, Professor at Department of Physics at NTNU.

A number of people deserves an acknowledgment for their support and help during the last semester. I would first of all like to thank my supervisor Ursula Gibson for being a fantastic supervisor who never stopped belief in my project. She always had her door open and helped me with questions and guidance both at the lab and in her office during the semester. I would also like to thank Irina Sorokina who measured my samples in the UV-NIR spectrum at the University of Vienna. Also a thank to Turid Worren Reenaas who contributed with the weekly discussion meetings where we could discuss our problems and statements. Other persons who deserve a thank is John Walmsley who helped me at the AES, Saepurahman who helped me with the NIR spectrophotometer, Julian Tolchard and Øystein Dahl who helped me with XRD, Hege Knutsen who helped me out on the Hall-measurement and my two partners at the reading room, Helene Hauge and Ragnhild Aurlien who helped med keep up my good mood.

I will also thank my wife, Ingeborg, and my son, Tobias, for letting me work at school when I rather should stay home and help them out. A thank-you also to family and friends who have been there for me whenever I needed something.

Contents

Abstract i

Preface iii

1 Introduction **1**

2 Theory **3**

2.1 Semiconductors 3

2.1.1 Doping 6

2.2 The pn-junction 10

2.3 The solar cell 14

2.4 The IBSC concept 16

2.5 Background research 21

2.5.1 ZnS 21

2.5.2 II-VI materials doped with Cr 22

2.5.3 ZnS:Cr and IB 23

2.5.4 Physical Vapor Deposition of ZnS thin films 25

2.5.5 Structural characterization of ZnS 26

2.5.6 Status of the IBSC concept 27

3 Experimental work 29

3.1 Deposition method 30

3.1.1 Physical vapor deposition, PVD 30

3.2 Characterization methods 33

3.2.1 Stylus Profilometer 33

3.2.2 UV-Visible-NIR spectrophotometry 34

3.2.3 Fourier-Transform InfraRed spectrophotometry 35

3.2.4 X-ray Diffraction 36

3.2.5 Auger electron spectroscopy 37

3.2.6 Hall measurement 38

3.2.7 Four probe measurement 38

3.3 Preparation methods 40

3.3.1 Building the lab 40

3.3.2 Sample preparation 41

3.3.3 Deposition 41

4 Results and Discussion 45

4.1 Deposition parameters and thickness measurement 46

4.2 Transmission spectra 49

4.3 Wide range spectrum 65

4.4 FTIR 66

4.5 XRD 67

4.6 AES 72

4.7 Hall-measurement and four probe measurement 75

5 Conclusion and future work **77**

Bibliography **80**

List of Figures **84**

List of Tables **91**

A Detailed balance of solar cell physics **95**

B Detailed balance of intermediate band solar cell physics **99**

C Pictures of the deposition system, "The Beast" **101**

D Datasheet, reflections of sapphire **103**

List of Abbreviations

AES	Auger Electron Spectroscopy
AFM	Atomic Force Microscope
CB	Conduction Band
EDX	Energy Dispersive X-ray
EPR	Electron Paramagnetic Resonance
ESR	Electron Spin Resonance
FTIR	Fourier Transform InfraRed
IR	Intermediate Band
IRSC	Intermediate Band Solar Cell
LED	Light Emitting Diode
NIR	Near InfraRed
ODMR	Optical Detection of Magnetic Resonance
PVD	Physical Vapor Deposition
SEM	Scanning Electron Microscope
S(T)EM	Scanning Transmission Electron Microscope
UV-VIS	Ultra Violet - Visible
VB	Valence Band
XPS	X-Ray Photoelectron Spectroscopy
XRD	X-Ray Difraction

Chapter 1

Introduction

The population on our planet is increasing and more countries are become industrialized. This increases the requirement for electric energy. It is desirable that this new energy comes from renewable sources with low CO_2 output and other greenhouse gases. Too high concentration of CO_2 in the atmosphere will contribute to the global warming. This again can lead to glacier meltdown, increase of sea level and change in animal- and plant habitats. This is a worst case scenario, but why risk our unique planet and ecosystems.

Electrical energy from solar cell is renewable [1, p. 182]. This energy source is also a non polluting energy source. The potential for solar cell are tremendous world wide, and the technology has in fact been one of the fastest growing in the world [1, p. 229-232]. When a solar cell is up working it is also silent. The installation is relatively easy and there is no need for large-scale arrays, the installation can be done directly on a house, car or of course at big power plants [1, p. 182].

The principle of photovoltaics came with the discovery of the photoelectric effect made by Edmond Becquerel in 1839 [2]. He observed that the voltage was light dependent for electrodes immersed in an electrolyte. The research of photovoltaics continued slowly and in 1954 the first practical silicon based solar cell was developed. This was based on single crystal silicon. It had an effiency of 6%, but soon it was increased up at 10% [3]. Since then solar power technology has been greatly improved and the effiency greatly increased. However, common solar cells, reffered to as *first generation solar cell*, even today normally opparates at 10-22%. The theoretically efficiency is

limited to 31% under unconcentrated light and 40.7 under full concentrated light [4].

In the beginning of the 1980's the research of thin film technology in solar cell started. This is called the *second generation solar cell.* Thin film technology has advantage over silicon wafers by reduced cost and bigger area which can work as cells. A disadvantage is the poor conversion factor at 5-10% [5, p. 4].

Third generation solar cells aim to combine high effiency with low costs. New concepts such as tandem cells, hot carrier cell, multiple charge carrier cell and IBSC are under investigation [5, p. 4]. The idea of an IBSC came from Laurent and Martí who in 1997 proposed to insert an intermediate band (IB) between the valence band (VB) and conduction band (CB) in the band gap. This makes room for a to step transition region. For this case the theoretical limit for unconcentrated light is 46.8%, and under full illumination the efficiency is limited to 63.1% [6]. If it could be possible to increase the number of sub-gaps in the band gap to infinity, the upper limit would be 86.6% efficiency [7].

In this study, the optical properties of Cr doped ZnS have been studied as a potential IBSC. Several samples with varying amount of ZnS:Cr were investigated. The samples were deposited through PVD with resistive heating. Some samples were deposited in room temperature, some were annealed for 2 h at 450 ^{0}C, and others were deposited on hot substrate to promote incorporation of Cr into the lattice. Afterwards the samples were characterized optically from UV-NIR, e.g. 250nm-2500nm. Some were also investigated in FTIR. The samples were analyzed in XRD and AES to find the lattice configuration. Four probe measurement and Hall-measurement were performed to determine the resistivity and the number of free carriers.

In chapter 2 the basic theory of semiconductors, p-n junction, the standard solar cell and the intermediate band solar cell principle is presented. The chapter also contains a section of previous work done on ZnS:Cr and IBSC. In chapter 3 there is a overview over the experimental methods which have been used, before the results and discussion are present in chapter 4. A conclusion based on my results, and a proposal of possible future work is presented in chapter 5.

Chapter 2

Theory

To understand how IBSC work it is necessary to have some basic background. In this chapter this background is given. The fundament of any solar cell is the semiconductor which is described first. To get current from excited electron-hole pairs, a p-n junction is needed, which is explained next. A presentation of the ordinary solar cell is then given before the concept and theory of the IBSC is presented. Also how to include an IB in a device is given. This chapter will also contains the challenges with IBSC and previous work made on ZnS:Cr samples.

2.1 Semiconductors

Semiconductors are a group of materials with electrical conductivity between insulators and metals. This is shown schematically in Fig. (2.1). The band gap for the insulator is to big so the electron can not be excited thermally or optically. For the case of the semiconductor the band gap is sufficiently small so there is a probability of excitation of electrons from the filled VB up to the CB by absorbing a photon. Pure semiconductor materials typically have conductivity between 10^6 and 10^4 $(\Omega cm)^{-1}$ at room temperature [8, p. 1]. Metals have a partially filled CB, or a total overlap between VB and CB so electrons can move freely around under influence of an electric field, leading to a high electrical conductivity. Some semiconductor have narrow band gaps, InSb around 0.18 e.V, while others, like ZnS, has a band

gap from 3.5 to 3.9 eV depending if the structure is cubic diamond or a mixture. Semiconductors with band gap around 3-5 eV are reffered to as wide band gap semiconductor [9]. For photon energies below the band gap energy the semiconductor is transparent for light [8, p. 324]. This gives a straight forward way of estimating the band gap of a semiconducting material.

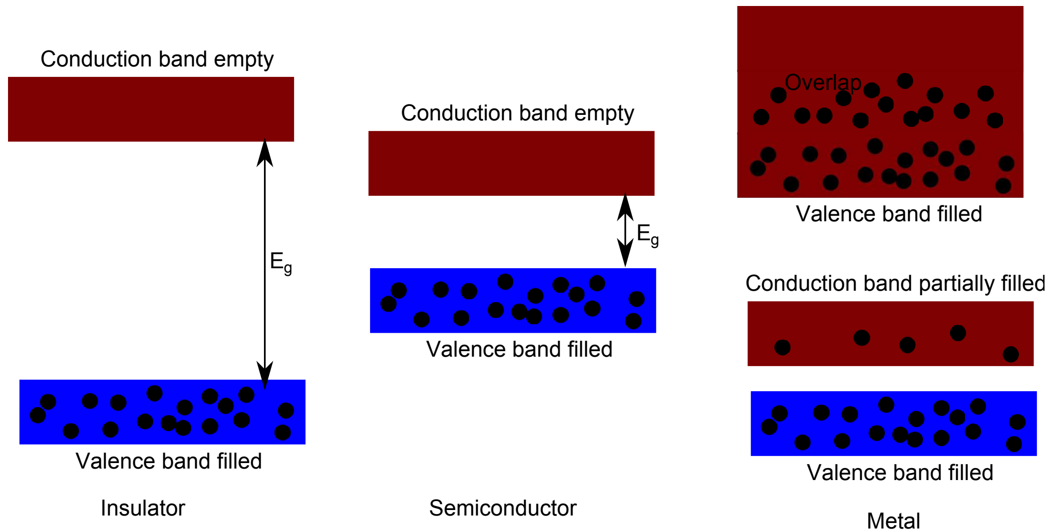

Figure 2.1: *Typical band structures for insulators, semiconductors and metals at 0 K. The insulator has a wide band gap so electrons can not get excited across. A semiconductor has a more narrow band gap so photons get excite the electrons across the band gap, while metals does not contain a band gap so they conduct easily* [10, Based on figure 3-4].

The semiconductors have in common that they share electrons to fill up their outer shell in covalent, or a mixture of covalent and ionic bondings. Semiconductors consisting of one type of atom are called elemental semiconductors. These are to be found in group IV in the periodic table and have covalent bondings. However, not all the semiconductors in group IV are elemental, for instance SiGe are not an elemental semiconductor even though both Si and Ge belong to group IV. Semiconductors can also be made by combining materials from group III and V, or groups II and VI. The materials found in these compounds are said to be binary III-V and II-VI semiconductors respectively and combine the covalent and ionic bondings [10, p. 64].

Electrons in solids obey the statics of the Fermi-Dirac distribution $f(E)$. At thermal equilibrium the distribution over allowed energy levels are given as

$$f(E) = \frac{1}{1 + e^{(E-E_F)/kT}} \tag{2.1}$$

where k is Boltzmann's constant, T the temperature, E_F is the Fermi energy and E the occupied state energy. The equation gives the probability of finding an occupied energy state at a certain temperature T. For semiconductors with energy equals the Fermi energy, $E_F = E$ the probability is equal 1/2, which can be easily shown. This is in the middle of the band gap, see Fig. (2.1). By increasing the temperature the last term goes towards 0 and the probability of finding a occupied state increases, e.g. in the CB. The factor kT at 300 K is though only 0.026 eV so even at room temperature the probability of finding electrons in the conduction band for a wide band gap material is minimal. For intrinsic semiconductors the Fermi level is denoted E_i.

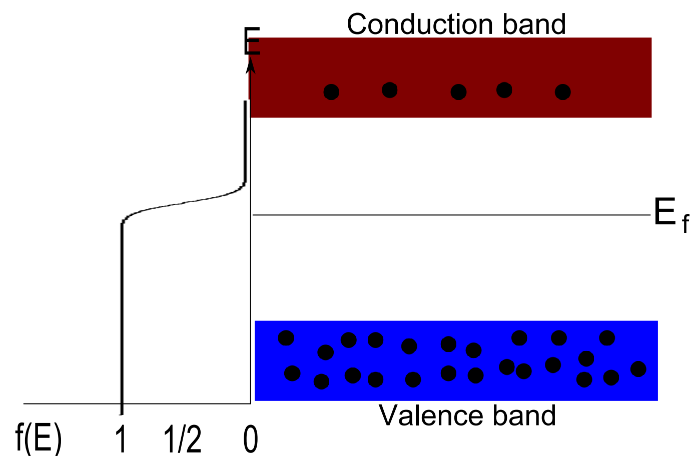

Figure 2.2: *The establishment of the Fermi-level in an intrinsic material. From the Fermi-Dirac distribution the probability of finding an occupied state with the Fermi energy is equal 1/2, making the Fermi-level in the middle of the band gap.*

At low temperatures the last term is dominating and only states in the lower VB are occupied, shown i Fig. (2.3(a)). By thermal or optical means electrons are given kinetic energy and can be excited to the CB across the forbidden band gap [10, p. 73], shown i Fig. (2.3(b)). This leaves behind a hole. When an electron absorbs a photon and excites to the CB it is called electron-hole pair generation. When the excited electron falls down to the VB again it is called recombination.

Semiconductors are also divided based on whether they have direct or indirect

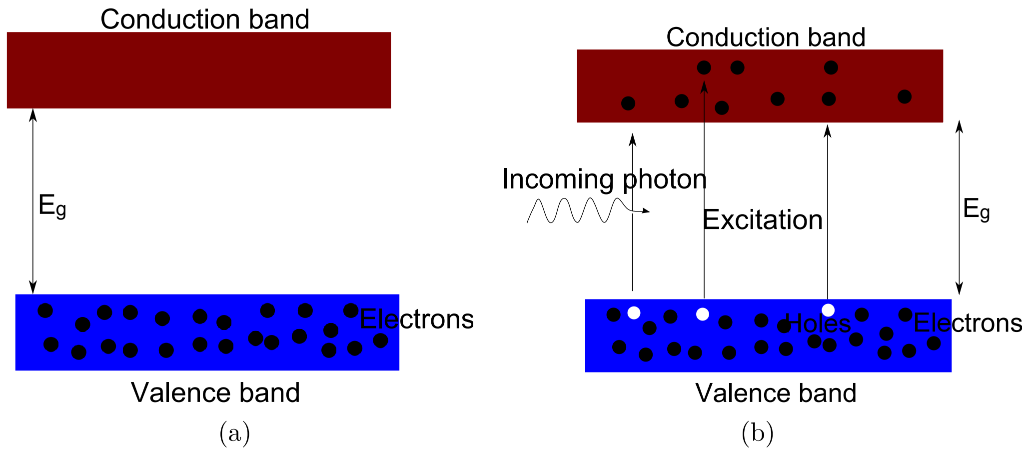

Figure 2.3: *The band alignment of a semiconductor at 0K in (a). In (b) electrons have been exited by absorption of photons, optical or thermal. The process is called an electron-hole generation.*

band gaps. The band gap is the distance between the energy bands, e.g. VB and CB. An electron is assumed to travel through a perfect lattice. The wave function of the electron propagate constant with wave vector **k**. If the wave vector is plotted vs. the allowed energy bands, e.g. VB and the CB, the bands will have a minimum and a maximum energy. If the semiconductor has a direct band gap it means that the maximum of the VB falls directly beneath the minimum of the CB, e.g. at the same **k** value, shown in Fig. (2.4(a)). If the maximum of the VB mismatch with the minimum of the CB the semiconductor has an indirect band gap, shown in Fig. (2.4(b)). An electron going from the VB to the CB in an indirect band gap must undergo a change in momentum for the electron. In general this causes radiation of heat rather than a release of a photon. When an electron falls from the CB to the VB in a direct semiconductor it will give off a photon with energy equal E_g. [10, p. 69].

2.1.1 Doping

Lets consider an ideally case e.g. infinite large crystal. Adding an electron as an impurity to the lattice gives an excess of electron in the lattice. This is done by introducing an atom from a higher group to the host material in the periodic table. The excess electron can move freely around in the lattice depending on the temperature. The extra electron is called a conduction

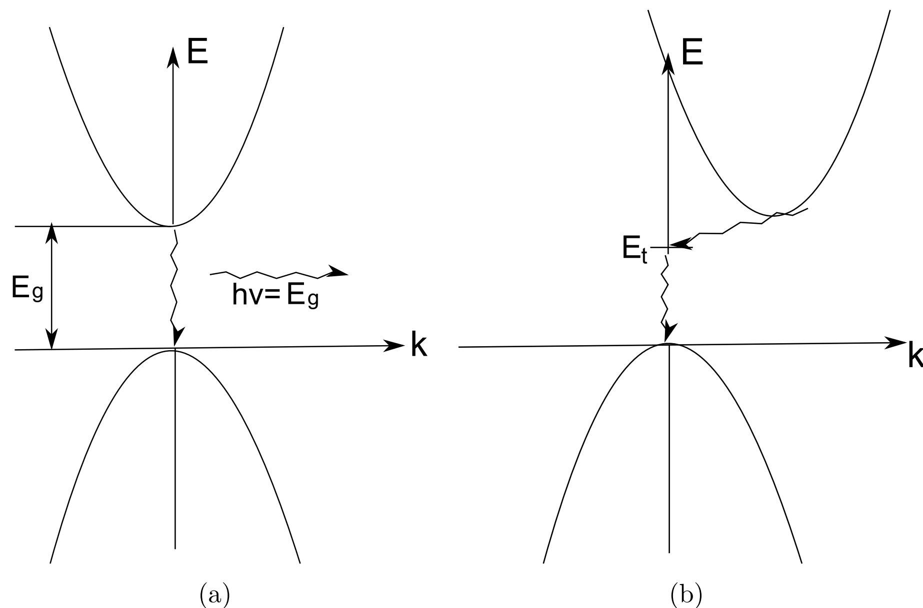

Figure 2.4: *The* ***k*** *space for an direct band gap in (a) and an indirect band gap in (b). The electron falling from the CB to the VB in (b) undergoes a change in the momentum.* [10, Based on figure 3-5].

electron [8, p. 4]. When there are excess free electrons we call the semiconductor n-type. The excess of electrons will create a level near the CB which will be filled at 0 K, see Fig. (2.5(a)). This will increase the probability for excitation of electrons from VB to CB by thermal or optical energy.

Another way to increase the conductivity is by introducing an atom from a lower group in the periodic system with one electron less than the host material. Electrons from the host material fill these states, leaving missing states or "holes" in the VB. The semiconductor is called p-type. By adding impurities from a lower group the impurity causes a level near the VB. This band will be empty at 0 K see Fig. (2.6(a)). The band can accept electrons easily at low temperature and is called an acceptor band.

If dopants have a large difference in the electronegativity, e.g. big deviation in number of electrons from the host material, they can form deep centers in the host material instead of an acceptor or donor level. The name stem from the fact that the energy levels are centered deep within the gap instead of close, either to the CB or the VB. A deep center can also be caused by defects in the semiconductor, such as dangling-bonds [11, p. 506]. These deep level impurities atom can act as both recombination centers or as traps

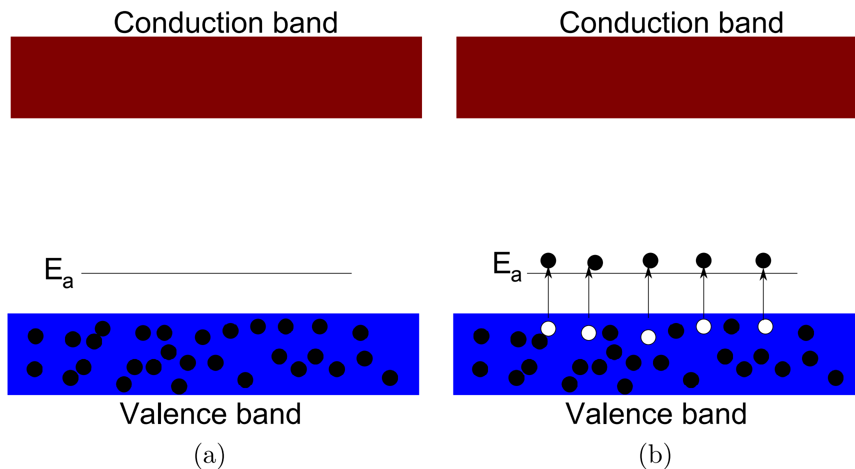

Figure 2.5: *A partially filled donor level is created near the CB at 0K by donor-doping. When the temperature increases the electrons can get excited easily across the band gap.* [10, Based on figure 3-12 (a)].

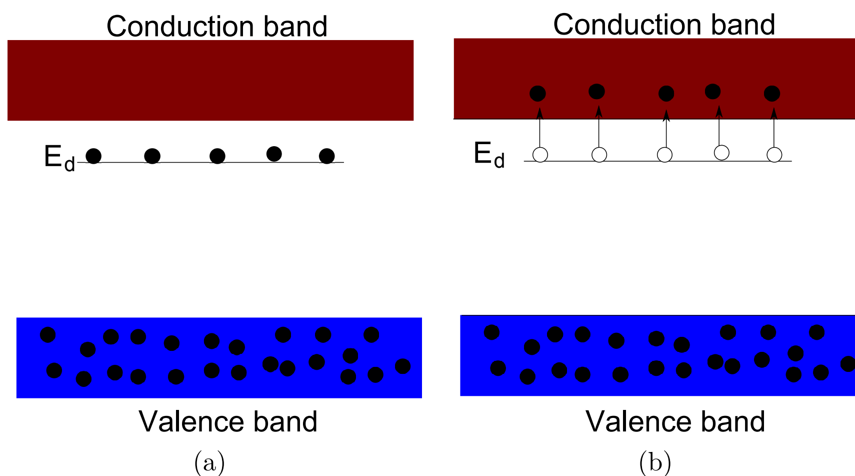

Figure 2.6: *A creation of an empty acceptor band created by doping in (a). (b) shows how electrons easily can excite up in the band, this can occur even at low temperature.* [10, Based on figure 3-12 (b)].

[8, p. 407]. A recombination center appears when there exist a dip in the CB at the same **k** value as a rise in the VB.

When changing the impurity concentration the Fermi-level will also be affected. By doping, as the concentration of holes are increased for n-doped material, the probability of finding an electron in the CB increases. This will move the Fermi-level closer to the CB, shown in Fig. (2.7(b)). For a p-doped material, the opposite occur. An absence of electrons decrease the probability of finding an electron in the CB moving the Fermi-level towards the VB. This is shown in Fig. (2.7(a)).

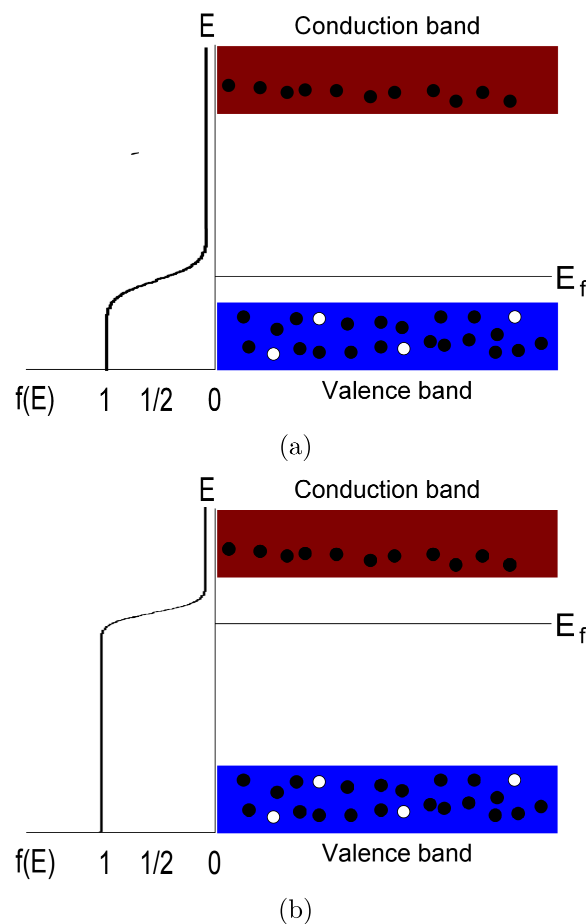

Figure 2.7: *The Fermi-level is dependent on the doping level in the material. (a) shows the Fermi level in a p-doped material, while (b) shows for n-doped material.* [10, Based on Figure 3-15].

2.2 The pn-junction

Semiconductors are used in several electric devices such as transistors, light emitting diodes, solar cell and lasers. The basis of all of these is the p-n junction. A p-n junction consists of one n-doped semiconductor and one p-doped semiconductor joined in a junction.

When a pn-junction is made electrons from the n-side will start to diffuse towards the p-side. The holes start to diffuse the other way. This causes charged area on both side near the junction. This will again put up an electric field from the n-side towards the p-side to stop the flow of electrons. The field starts drifting electrons the other way. A steady state is reached when the drift and diffusion of electrons and holes are equalized [10, p.171]. The zone where the drifting and diffusion occurs is called the depletion region. This region stretch out equally in both materials if the doping concentration is equal for the p and n material. Figure (2.8) shows a depletion region for a p-n junction. If one side is heavily doped compared with the other side the depletion region mainly extends into the less doped side.

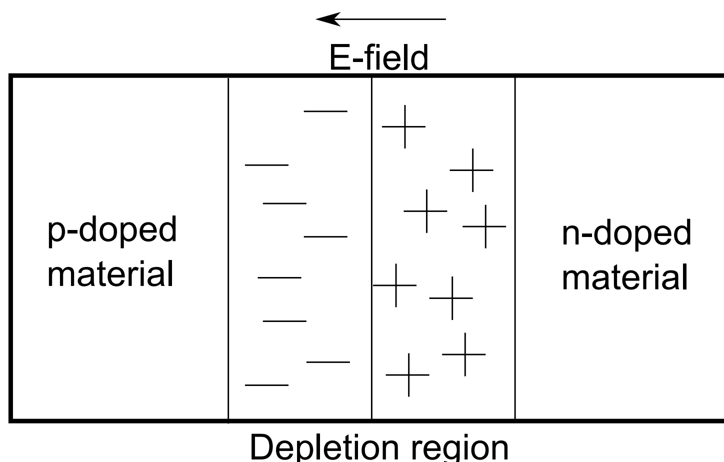

Figure 2.8: *Schematic of the depletion region and how an E-field are established when a p and n material is junctioned together.*[10, Based on figure 5-11].

Before the p-n junction is made the Fermi-level is aligned closest to the CB or VB depending whether the semiconductor is n or p doped respectively. This can be seen in Fig. (2.9(a)). When a p-n junction is made the Fermi level stays constant through the junction occuring a band bending of the valence

and CB shown in Fig. (2.9(b)). A depletion region is put up where the band bending occur. When the junction is exposed for an external voltage, or excitation of electrons, an excess of carriers, e.g. holes or electrons, in the conduction or VB respectively will appear. This is because not all energy from the cell will be extracted. This causes higher energy for electrons on the n-side in the CB than the electrons in the VB on the p-side, which lead to division of the Fermi-levels into quasi-Fermi levels. The voltage of the cell is the difference of the quasi-Fermi-levels divided by the elementary charge. The quasi-Fermi-levels are denoted E_{Fn} and E_{Fp} respectively, see Fig. (2.9(c)) [4].

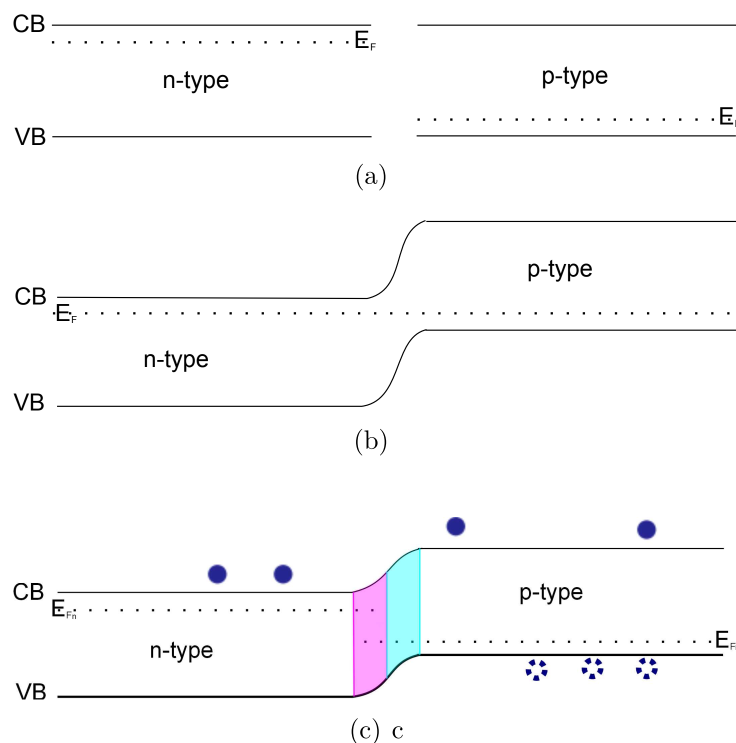

Figure 2.9: *Creation of a pn-junction and the affection on the Fermi-level and the band alignment. (a) shows two opposite doped semiconductors before the junction is established. (b) shows the band bending to keep the Fermi level constant throughout the system, while (c) shows how a depletion region and quasi-Fermi levels are established.* [4, Based on Figure 2.6].

If the p and n side is based on semiconductors with equal band gap the junction is called a homojunction e.g. p-n junction within a single semiconductor. The creation of a homojunction is shown in Fig. (2.9).

Figure (2.9) is in an ideal case where the band gap is constant across the junction. In reality this is not always the case. Often the p-n junction consists of different doped semiconductors with different band gaps. This is called a heterojunction. The heterojunction is most used and appears in field-effect transistors, lasers and bipolar transistors. An illustration of a heterojunction is given in Fig. (2.10). If the difference between the two band gaps from the p- and n- doped materials are big enough, the Fermi level in the wide band gap material can be above or beyond the CB or VB respectively. If this happens it is resulting in a discontinuity in either the VB or the CB so the Fermi level stays constant through the material.

A p-n junction at zero bias has a built-in potential at equilibrium condition. However, the band bending, potential barrier and the depletion width can be strongly influenced by an external voltage [10, p. 180-184]]. If the junction is exposed for a forward bias the width of the depletion reduces. This also reduces the potential barrier and the band bending. As the voltage increases the built in electric field can not counteract the applied voltage and the resistance of the material decreases.

Electrons exposed to thermal heating, battery or light can be used to excite electrons from the VB up in the CB. This way the p-n junction can be utilized in transistors, light emitting diodes (LED) and as a solar cell. In LED, light emitting diode, an external circuit is used to excite electrons up in the CB. During relaxation a photon is given of with a certain wavelength. The solar cell works in the opposite direction. Here photons from the light excites electrons which are utilized by an external circuit.

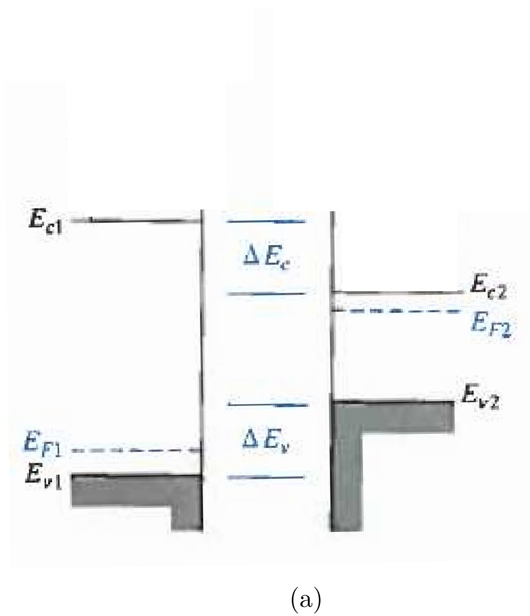

(a)

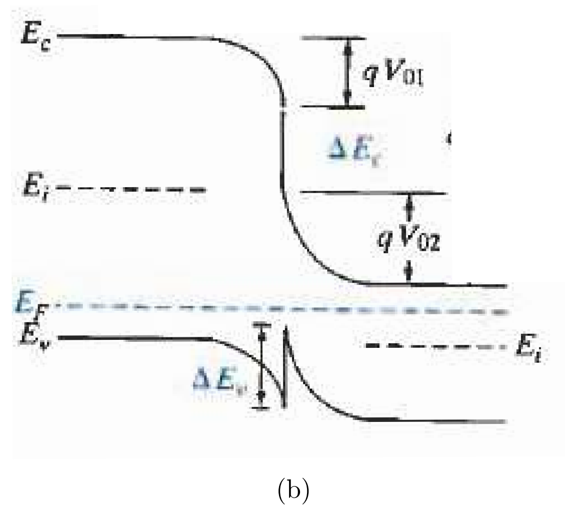

(b)

Figure 2.10: *An ideal heterojunction between a wide band gap p-type material and a more narrow n-type material. Figure (a) shows the bands before they are aligned. As can be seen the Fermi level of the p-type material is below the VB for the n-type material. This is also shown for the band alignment in (b). Discontinuities in the conduction and VB are created for the Fermi-level to be constant.* [10, Based on figure 5-45].

2.3 The solar cell

In a solar cell, e.g. photovoltaic cells, electric energy is transformed directly from sunlight. This occurs as electrons are excited from a low energy state to a higher energy state from an incoming photon. To extract the electric energy the solar cell has to be coupled to an external circuit in a properly way before the excited electrons are back in the ground state. For a photovoltaic cell it is essential to generate electron-hole pairs without recombination. This is done by applying an external field driving the holes and electron in opposite directions and then let the electron go back in into the VB, shown schematic in Fig. (2.11).

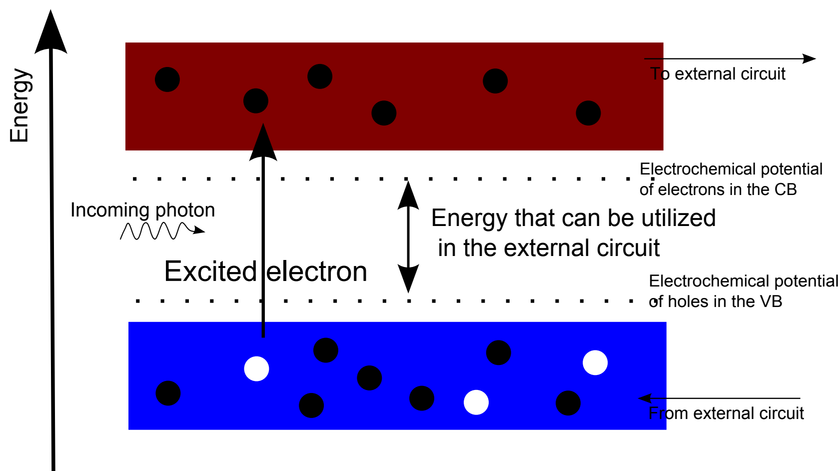

Figure 2.11: *Excited electrons can be utilized in an external circuit to create current flow. An incoming photon excites electron from the VB to the CB. Excited electrons is driven to an external circuit and back to the VB. The gap between the electrochemical potential in the VB and CB is the limit of extracted current.* [4, Based on Figure 2.2].

To calculate the efficiencies of photovoltaic effects the detailed balance theory is an widely used concept [4]. During calculation only the fundamental physical effects are taken into account. For a solar cell these effects are the absorption and emission of photons. The detailed balance approach is given in Appendix A. To extract more energy from the absorption process the separation between the chemical potentials have to be increased. This can be done by not extracting the electrons from the CB immediately after excitation. The drawback is that with increased electrochemical potential the re-combination of electron-hole pairs increases as the time increases. The

electrochemical potential are also reffered to as quasi-Fermi levels [4].

Each electron in the CB which is not recombined will deliver energy to the external circuit. As mentioned, when the voltage increases the recombination also increases. There is therefore a best match between the quasi-Fermi levels and the highest effiency you can get out of the solar cell. For a single band gap solar cell this efficiency is limited to 31.0% under 1 sun and 40.7% under concentration of the hole hemisphere, e.g. 46050 suns.

It is important that the limited efficiency is what can theoretically be extracted. Common solar cell, of Si, with a band gap at 1.1 eV is operating with a much lower effiency, for instance at 16% effiency. The highest efficiency achieved from a Si single crystal solar cell is 25% [1, p. 201 and 207].

There are several losses contribution to the rather poor efficiency of a single gap solar cell. Figure (2.12) shows how electrons are excited by an incoming photon from the VB up in the CB through the band gap. Photons with energy lower than the band gap continue through the material (1). Photons with energy equal the band gap excites the electron without losses (2), while photons with excess energy (3) give off heat in the relaxation within the CB.

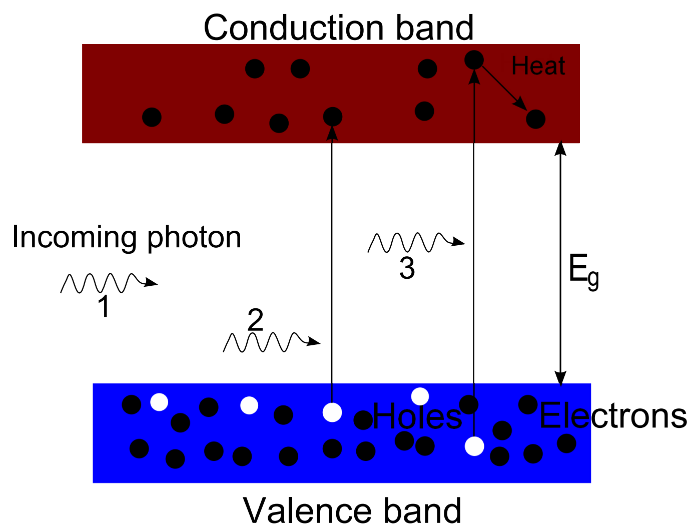

Figure 2.12: *How photons interacts with electrons and excite them in the CB. Photons with less energy than band gap energy (1) continue through the material, photons with energy equal band gap energy excite electrons without losses (2), while photons with energy above band gap energy undergo heat exchange in the relaxation within the CB (3)* [4, Based on figure 2.5].

From Fig. (2.12) the two main losses are shown. Excess photon energy lost from short wavelengths account for 33% alone. Photon energy with energy less than band gap energy leads to 23% loss, while other losses like recombination of electron-hole pairs reduce the efficienct with 4%. Other losses are [1, p. 200-207]:

- reflection of photons at the cell surface
- voltage factor because of the separation in the quasi-Fermi level
- curve factor as the solar cell is strongly influenced by the p-n diode and the output voltage

Since only light of energy higher than the bandgap, e.g. E_g>hν can be utilized, a Si cell will not be able to utilize radiation above 1127nm. Also high energy in the visible region will not be utilized, still Si cells can utilize 2/3 of the solar spectrum. The solar light spectrum at the top of the atmosphere coincide well with a black body spectrum at 5250 K, seen in Fig. (2.13), which is the temperature at the surface of the sun. The red area is due to absorbing gases in the atmosphere. As can be seen the high intensity is in the visible light region, while it drops off in the infrared and ultraviolet directions. The solar cell should therefore also be designed to utilize light in the high intensity region. This is considered when new solar cells are investigated by making use of tandem cells or semiconductors with a wider band gap and introduce them for an IB.

2.4 The IBSC concept

In 1997 a new solar cell concept appeared. This was the idea of an IBSC invented by Luque and Martí [6]. The idea was to insert one IB between the VB and the CB. For one extra band the theoretical efficiency is raised to 63.2% under full illumination. A convential single gap solar cell has a theoretical efficiency under full illumination at 40.7%. For both cases the conditions are the same, considering the cell lattice temperature at 300K, the illumination comes from an isotropic gas at 6000K, no ohmic losses and the case that any non-radiative recombination is suppressed [12]. To achieve the lattice temperature at 300K under these circumstantials sounds unlikely though.

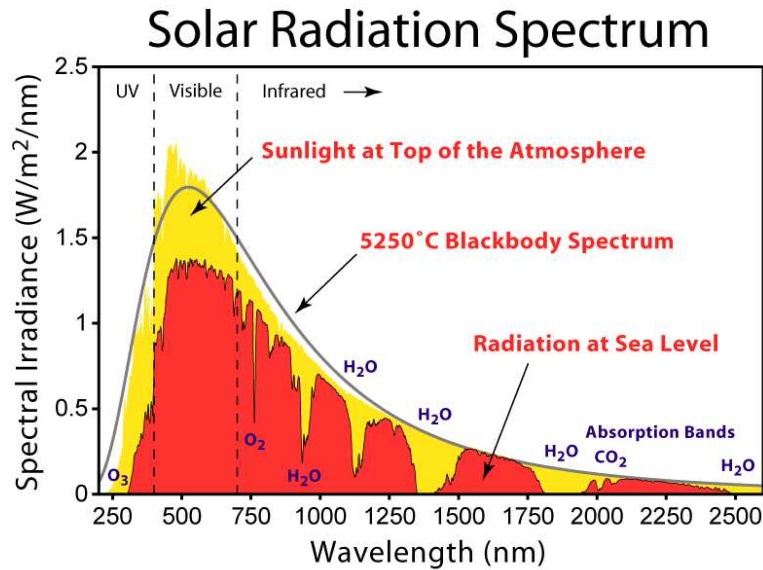

Figure 2.13: *Black body radiation from a 5250 ^{0} C surface, black line, the sunlight at the top of the atmosphere, the yellow area and the incoming radiation at the sea level, the red area. The figure also shows the absorption band for H_2O, O_2 and CO_2.*

However, for unconcetrated light the efficiency limit is 46.8%, which also is a tremendous improvement from the convential single gap solar cell at 31% [4]. A detailed balance approach for the IBSC can be seen in Appendix B.

IBSC are based on the ordinary pn-junction, but with one main difference. Between the VB and the CB there is a band of electron states. This allows electron to get excited from the VB to IB, from IB to CB and VB to CB see Fig. (2.14). The utilization of a broader spectrum is achieved at the same time as a semiconductor with a wider band gap is used so that high energy photons also can be utilized.

Common Si solar cells absorb all radiation below 1127 nm and have in fact a band gap which is around the optimum band gap for a single junction solar cell (1.12 eV) [12]. A wider band gap implies a more narrow spectrum range. But with an extra band within the band gap, the excitation of electrons can occur in a two step procedure. And this way also catch up the low energy photons and utilize more of the high energy photons. Figure (2.14) shows how the excitation can be in an IBSC system. The first step (1), is for photons E_3>hν>E_1 which excites the electron from VB up to IB. The next

step (2) is E_3>hν>E_2 which excites the electron from IB up to CB, where it can be utilized. For electrons where hν>E_3 the electrons can get excited all the way up to the CB (3). The best match between VB and IB is 1.42 eV and 0.67 eV from IB to CB [4].

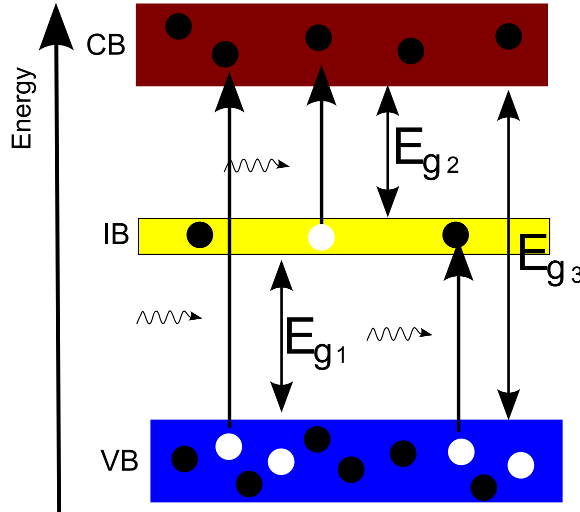

Figure 2.14: *Shows the to step transition of the excitation. The excitation from the VB to the IB, labeled E_{g1}, from the IB to the CB, labeled E_{g2}, and from the VB to the CB, labeled E_g3.* [4, Based on Figure 3.1].

For a IBSC to work, there are some key requirement that must be fulfilled [13]. For photovoltaics to reach a high efficiency as possible the radiative recombination must be predominately. An IB shall not extend through the whole device, like the VB and CB. This causes the radiative recombinations to exceed the non-radiative one. The IB will prevent the intermediate electronic states from becoming non-radiative recombination centers [13]. As the radiative recombinations becomes the dominant the lifetime of recombination between the three bands exceed the carrier relaxation times within each of the three bands. A deviation from the single gap solar cell the IBSC has three quasi-Fermi levels when it is up working, E_{FC} for the CB, E_{FI} for the IB and E_{FV} for the VB, see Fig. (2.15). The IB material will then be sandwiched between one p-doped material and one n-doped material making a p-i-n junction. The two doped materials separate the IB material and the contacts. This way no current can be harvest directly from the IB [13]. The ordinary p-n junction will act as an contact for electrons from the CB and holes from the VB to the external circuit, and make the generation of electric current. The maximum output which can be extracted is the voltage differ-

ence between the CB and the VB quasi-Fermi levels at the p- and n-contact. This is therefore limited by the band gap of the host material, E_G, and not by the sub-band gaps. For the IB to excite electrons from the VB to the IB, and from the IB up to the CB, the IB should ideally be half filled. This way there will always be empty states for electrons to be excited, but also electrons that can excite. For this to occur the quasi-Fermi level for the IB E_{FI} has to be within the the IB. This applies also for non-equilibrium conditions [13].

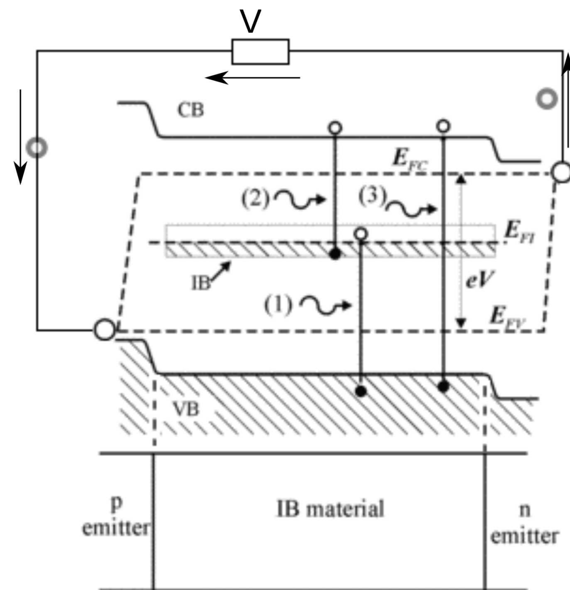

Figure 2.15: *Shows the quasi-Fermi levels for the CB, VB and IB. It also shows the three excitation possibilities and the direction of the utilized voltage.* Based on figure [12, 1(b)] and [13, 1(b)].

The thickness of the material hosting the IB is also an issue. In the p-i-n junction, the i-layer is the most insulating one. As the p- and n- layers inject holes and electrons the carriers must go through the i-layer. One way is by tunneling through the barriers under high electric field. Another way, which plays a more minor role, is by "thermionic emission" [14]. This happens because of the creation of notch barriers at the interfaces between the p-i layer and the i-n layer. If the carriers thermal energy is larger then the barrier height the carriers can flow over the barrier. This is though a minor chance to occur because of the large difference in the band gap for the doped layers and the intrincic one. The major injection of carriers is therefore from tunneling. It is therefore to believe that the carrier injection will be strongly limited by the thickness of the i-layer. However, Kruangam et al. showed

that an i-layer of 500 Å had the highest electroluminescence compared to samples of thicknesses 250 Å, 750 Å and 1000 [14].

IB material candidates

So far there are no common IBSC available, however there are in general two ideas for making IBSC, e.g. Quantum dot IBSC, and bulk IB-materials. Recent reports demonstrate a bulk IBSC, but with a rather poor efficiency, less than 1% [12]. In this report the bulk material ZnS:Cr is investigated so I will examine the principle here.

In a bulk IB-material impurity atoms are used to make an IB in a host semiconductor. The idea is to introduce the semiconductor for impurity of high concentration to make delocalized states so an IB can be formed from electron states, rather than single impurities that will have localized states [4]. A localized state will work as a center for non-radiative recombination, while the delocalized states will prevent the non-radiative recombination. To form a transition where electron states can take place a impurity density of 10^{20} cm^{-3} is required [4], which is about 0.1%. When the research of the IB concept startet, in 1997, the existence of a material with possibilities of making a deep trap was considered as improbable. However it is clear that deep trap levels are created when the concentration of impurities are of a certain value, which may produce IB with reduced non-radiative recombination. Compared to quantum dots IBSC the advantage bulk IB materials have is the stronger possibility for sub-band gap photon absorbtion because of the high density of impurity level. For the case of the quantum dots IBSC it is the weak absorption which causes the poor efficiency [12].

Thin-films

Thin films are used as anti reflecting coating on common single gap solar cell [1, p. 203]. This way as much as possible of the incident solar radiation can be harvested. Thin films can also offer significant flexibility for the fabrication of homogeneous IBSC [12]. For thin films deposition in PVD the choice of host and impurity can be made in wide range. Also during fabrication variables like thickness, rate and concentration are easy to change for the best composition. Thin films are suitable for a wide variety of analytical

techniques to determine the optical activity of the material.

2.5 Background research

In this section background research on ZnS:Cr thin films will be presented. This way the results from the investigation can be compared to previous work. The section starts out with some basic about ZnS before II-VI materials doped with Cr is discussed. Then different ways of depositing ZnS:Cr thin films and structural characterization of them are described. At the end a short presentation of the status of the IBSC research is given.

2.5.1 ZnS

ZnS is a wide band gap direct semiconductor. The material consists of Zinc, Zn, and Sulfur, S, which make ZnS an II-VI compound [10]. The band gap varies depending on the structure. The two natural ways ZnS organizes is in zinc blende e.g cubic, and wurtzite e.g hexagonal, structure, see Fig. (2.16). The band gaps are 3.84 eV for the cubic form and 3.94 for the hexagonal form at low temperature. The lattice constant is 5.41 Å for the cubic form while the a-axis is 3.81 Å and the c-axis is 6.23 Å for the hexagonal form [15]. In equilibrium, at high temperatures, e.g 1020° C zinc blende converts to wurtzite structure [16]. ZnS also appears in so-called mixed-polytype structures, and is therefore one of the richest chalcogenides compounds, structurally speaking [17]. ZnS has extremely good optical quality and is a widely used semiconductor. It can be used as a dielectric filter in the visible range or as a reflector because of the high refractive index of 2.35. It is also used in flat panel displays, injection lasers and light emitting diodes [18]. Theoretically it has been shown that ZnS doped with transition-metals, such as Cr, Fe and Ni can become half metallic, ferromagnetic and 100% spin polarized at the Fermi energy from density of states [18]. This makes ZnS a good candidate, as the host, for an IBSC. The band gap is wide enough so electrons can get excited across the band gap at the same time a two step transition can occur through the IB.

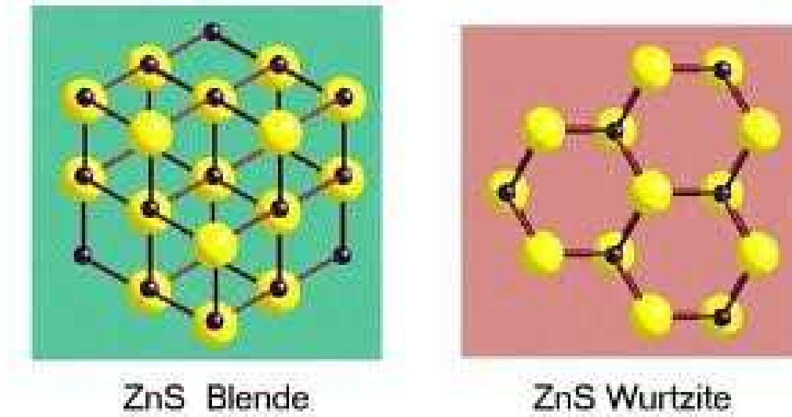

Figure 2.16: *The two main structure of ZnS, sinc blende (left) and wurtzite (right).*

2.5.2 II-VI materials doped with Cr

In the early 1960's interest in II-VI compounds semiconductors with transition-metal doping from Cr^{2+} increased [17]. Especially since the mid 1990s ZnSe:Cr is a widely studied material for their laser possibilities. The similarity to ZnS, which also is a II-VI compound, is big. However, ZnS:Cr is mainly studied as an model object in spectroscopy. One reason for this can be the wide band gap for ZnS, which has been reported at 3.8 eV vs. 2.8 eV in ZnSe [17]. Most of the research is in relation for lasers. The reason is due to the fact that Cr^{2+} work as an luminescence killer [17][19][20], e.g. the electrons falling from CB towards VB get captured by the Cr and an IR light is sent out instead of a UV light. A broad absorption band occur around 1.7 μm as shown in Fig. (2.17) [17]. This gives rise for a broad tunability in the laser operation, actually over a 1100 nm broad spectrum.

To make ZnS:Cr compound with IB the goal is to substitute the Zn^{2+} with the Cr^{2+} forming a $Zn_{1\text{-}x}Cr_xS$ compound. To achieve such a structure the Cr atom, $Cr(3d^54s^1)$, will replace the cation atom in the tetrahedral lattice configuration. The field of the host crystal, ZnS, splits the $Cr^{2+}(d^4)$ free ion ground state into ^5E orbital doublet and $^5T_2$ orbital triplet. The latter can further split making possible transition from $^5B_2$ and ^5E, while ^5E can split into $^5A_1$ and $^5B_1$ [21].

The absorption at 1700 nm, Fig. (2.17) is due to the transition of $^5T_2$ excites

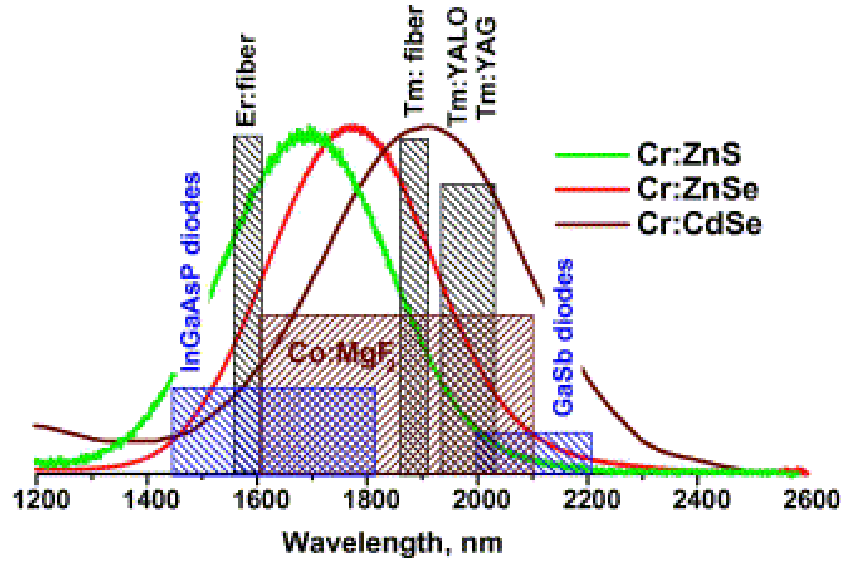

Figure 2.17: *An absorption spectrum of ZnS:Cr, ZnSe:Cr and CdSe:Cr. The absorption of* Cr_{2+} *in ZnS appear at 1700 nm. The figure is taken from* [17].

to ^{5}E state for the Cr^{2+} ion. This is the only allowed spin transition in the system [17].

2.5.3 ZnS:Cr and IB

There exist several reports showing that ZnS:Cr hosting an IB [17][20][22][18], which is the reason for quenching of the luminescence. Naturally occuring defects in pure ZnS alone has a trap distribution at 2.18 eV [22]. Introducing Cr can introduce an IB at other levels in the band gap. Nelkowski et.al. reports a deep trap in Cr:ZnS at 0.74 eV due to Cr^{2+} which is filled by excitation during illuminating with UV light [20]. Other reports that lattice defects in the band gap, making traps, are created at different energy levels when the Zn^{+} is substituted with Cr^{+} or Cr^{2+} [23]. From Fig. (2.18) it is shown that Cr^{+} defects occur at 1.8-2.2 eV and 2.6-2.7 eV from the conduction band edge. The former associated by a donor, and the latter a defect caused by an isolated acceptor. For Cr^{2+} the defects caused by an isovalent trap appear at 3.5 eV. Peaks due to optical ionization are shown at 1.3-1.5 eV for Cr^{+} and at 2.8-3 eV for Cr^{2+}. The photorecharge by $Cr^{2+} \rightarrow Cr^{+}$ takes place for any process generating free electron and not just the direct transition e_{VB} $\rightarrow Cr^{2+}$. In the cited work two 650 nm thick thin films were made containing

0.2% and 2% Cr by e-beam evaporation.

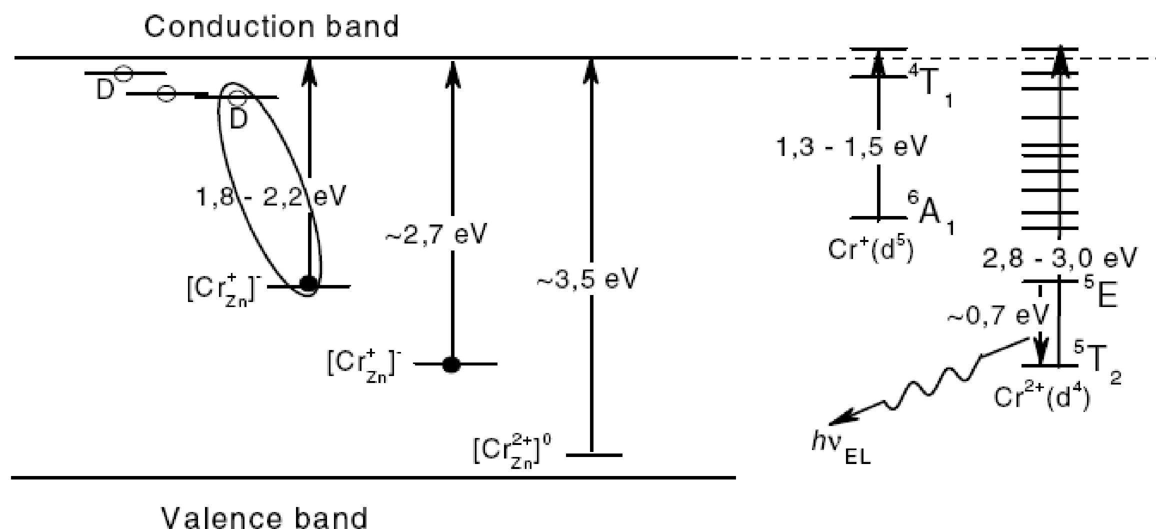

Figure 2.18: *Lattice defects for Cr substituted with Zn. The different Cr^{2+} and Cr^{+} ions shows traps and levels at different energy levels within the band gap. The energy levels can work as transition places for an IB between the valence and CB. The figure is taken from* [23].

As several reports showing that ZnS:Cr having an partially filled IB [19][20][22][18] the idea of using Cr:ZnS in an IBSC material has arisen [24]. This has been investigated theoretically based on the density functional theory. Two Cr atoms have been substituted with two Zn atoms in a 64-atom cubic cell. The Cr atoms were placed as far from each other as possible. The equivalent doping level was 3.125%. The results show that uniformly Cr doped ZnS has a partially filled IB. This is true for both ferromagnetic and antiferromagnetic spin alignment [24].

Even though Cr:ZnS has shown promising properties for hosting an IB, major challenges still remain. One challenge is to get ohmic contacts to an insulating ZnS crystal without changing the crystal properties [25]. Another is the difficulties attached to making p-n junctions. As the concentration of impurities from Cr increases in the ZnS the mobility also shows decreasing effects. Another issue is the fact that ZnS is not a good conductor, at least not at room temperature [19]. The doping level of impurities is also an important issue. It is shown that a doping level up to 0.1 mole % will increase the conductivity, but above this limit the conductivity falls off. The problem

is to make a continius IB with such a low amount of Cr.

2.5.4 Physical Vapor Deposition of ZnS thin films

Physical vapor deposition by resistive heating is an easy way of making thin films. Pure ZnS has shown good response on deposition with resistive heating. Keeping the rate of ZnS below 5 Å/s the thin film of ZnS will give negligible absorption [26]. Deposition in room temperature at low pressure and relative high rate has shown refractive index of 2.4 as bulk value. The band gap found under these circumstances, which is in the range 3.51 - 3.84 eV, shows good correlations to other growth technique. Nadeem et.al. reports on defects in the thin film implying structure defects caused by deposition in room temperature. The possibility for states in the band gap [26] is also mentioned, although the density of these levels would be difficult to control.

Adding Cr to the ZnS and making them substitute the Zn can be done several ways. One is with resistive heating of both Cr and ZnS, with both sources operating at one time. To overcome the fact that Cr can bond to each other before they get substituted with Zn atoms the deposition can either be made with a hot substrate or post-deposition annealing. In Vlasenko et.al. a doped Zns film was made with e-beam evaporation of ZnS and evaporation of Cr by resistive heating. The concentration was $> 20^{20}$ cm^{-3}. The sample was annealed afterwards at 550^0C for 1 h. The samples showed absorption band for the $Cr^+ \rightarrow Cr^{2+}$ transition.

A third way of depositing ZnS:Cr is on a hot substrate. If the substrate is hot the reaction between Cr and ZnS can occur during deposition at the substrate. ZnS evaporated onto substrates in the range of 200^0C - 350^0C has been investigated showing best result for the 300^0C deposition. For this case pure cubic crystal is reported with a band gap of 3.61 eV. At 300^0C the ZnS configuration showed equal amount of Zn and S, e.g. stoichiometric structure. Above 350^0 the ZnS thin film showed places with amorphous structure [27].

There exist reports showing that amorphous structure of ZnS thin films growth by chemical bath deposition often occur. Contamination of ZnO or Zn(OH)2 are also a existing problem. By annealing the samples for 400^0C this problem has been solved according to [28]. Other reports of creation of ZnO when annealing ZnS for 3 hours at 500^0 [29]. This creation did not appear for 450^0C and 400^0C, see Fig. (2.19). Apparently this comes from the

fact that during deposition a small amount of O has been trapped in the thin film, concluded from Energy Dispersive X-ray spectroscopy (EDX). During annealing the O is driving further in to the thin film and make substitution with S creating ZnO.

2.5.5 Structural characterization of ZnS

XRD has been reported on ZnS thin films grown by E-beam evaporation for several samples with different thicknesses [29]. Samples with thicknesses 290 nm and 400 nm show two peaks for the (111) and (220) configuration, see Fig. (2.19). The 400 nm sample was also annealed at 400^0C, 450^0C and 500^0C for 3 hours. This corresponds to a cubic structure. The peaks decrease with decreased thickness of the thin film. However, for the annealed sample the peaks grew bigger with increased temperature. For the sample which was grown at 500^0C Zn combined with O and formed ZnO in the sample. The 50 nm sample does not show peaks at all which implies amorphous structure.

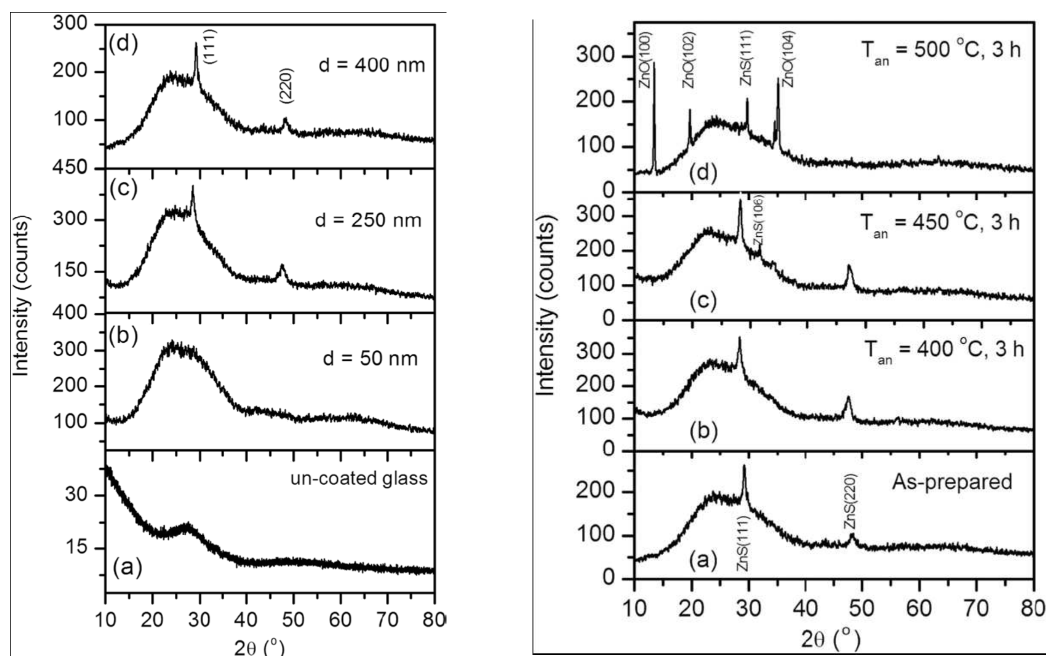

Figure 2.19: *Diffracted peaks for ZnS films made with E-beam evaporator. The left figure shows the diffraction pattern for different sample thicknesses. The right shows how annealing effects the sample of 400 nm. Figure taken from* [29].

ZnS grown by electrodeposition from zinc chloride and sodium thiosulfate making thin films on indium tin oxide glass substrate has been investigated in XRD [30]. The films were in the range of 190 - 600 nm and are grown by a deposition potential of -1V, -1.1V and -1.3V for 15 minutes. The spectrum is shown in Fig. (2.20).

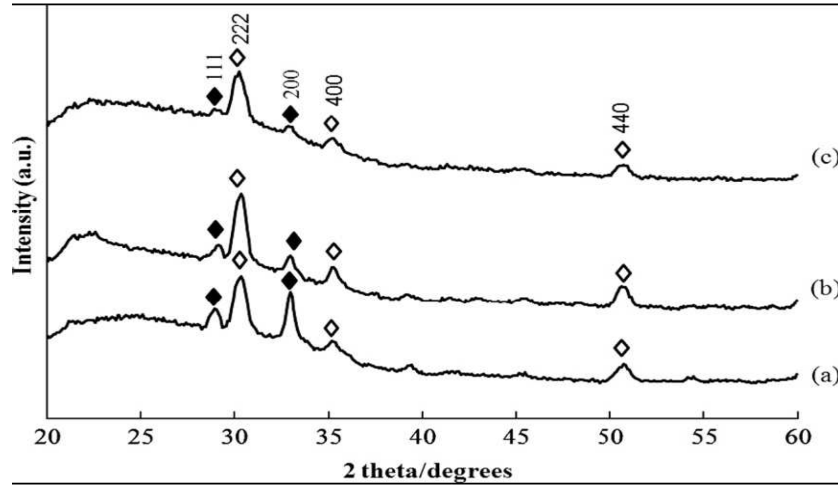

Figure 2.20: *XRD plot of ZnS deposited by electrodeposition for 15 minutes. The white markers show the diffraction from the substrate,* $In_{1.875}O_3Sn_{0.125}$. *The black markers show the diffraction from the ZnS. The revealed configurations imply cubic structure. Graph (a) is from the film grown at -1V potential, graph (b) was grown at -1.1V and graph (c) for the film grown at -1.3V. Figure taken from* [30].

The films were deposited with electrochemical bath in room temperature. The 2θ scan shows peaks for the (111) and (200) configuration. Further results from XRD at other samples deposited under same conditions, but at longer deposition time imply a cubic structure. Characterization performed with atomic force microscope (AFM) in the same report also support this assumption [30].

2.5.6 Status of the IBSC concept

For IBSC bulk materials both III-V and II-VI oxide semiconductors are being investigated. A promising candidate is O doped ZnTe which showed an increase of 50% in the efficiency compared to the reference cell from ZnTe. The energy level from O is stated 0.2 eV below the CB. [12].

Another way of implementing an IB is by quantum dot implementation. Quantum dots are made by inserting nanoparticles or droplets in a material, often with a higher band gap. By n-doping in the barrier the quantum dots can make a half-filled IB with possible transition from the VB and to the CB. Quantum dots solar cell is the most investigated area for the IBSC. However, the results from InAs/GaAs quantum dots solar cells have shown less efficiency then expected, consider the non-optimal band gap which GaAs hosting. [12].

Chapter 3

Experimental work

To characterize the deposited samples made in this thesis different techniques at both NTNU and Vienna were performed. To determine the chemical and physical structures of the samples XRD and AES have been used. The electrical properties were found by Hall-measurement and four-probe measurement. The result was also confirmed from AES. The optical properties were found by optical transmission spectroscopy, and the thicknesses of the samples were re-examined with profilometer. A picture of the deposition system is shown in Appendix C.

In the beginning of this chapter the physics behind the physical vapor deposition method is presented. Then a description of the characterization methods which have been performed in this thesis, the type of the instrument and where the measurement was performed, is given. At the end the description of how the samples were prepared and deposited is described.

3.1 Deposition method

3.1.1 Physical vapor deposition, PVD

This section is a summary of chapter 5 in [31].

Physical vapor deposition is a generic term used for several applications such as sputtering, E-beam evaporation and resistive heating. For my review it is the latter case we will look into. To make a thin film using resistive heating as PVD we need a vacuum chamber. This way the thermal vaporized source reach the substrate without collision with other molecules or residual gas within the deposition chamber. Vacuum deposition requires a vacuum better than 10^{-4} Torr. Even with this pressure there will exist unwanted residual gases that can contaminate the film. A better vacuum will give a less contaminated film.

Since vacuum is needed the method is also called vacuum deposition. This is the most widely PVD deposition process used. The applications of this method include among others deposition of:

- electric conductive coating
- optical coating
- insulating layers
- corrosion resistant coating

During evaporation atoms are going from the source towards the substrate, hopefully without any collision. The rate of evaporation can be given from the Hertz-Knudsen vaporization equation, Eq (3.1)

$$dN/dt = C(2\pi mkT)^{-1/2}(p^* - p)sec^{-1} \tag{3.1}$$

where dN=number of evaporating atoms per cm^2 of surface area, C=constant that depends on the rotational degrees of freedom in the liquid and the vapor, p^* = vapor pressure of the material at temperature T, p=pressure of the vapor above the surface, k=Boltzmann constant and m=mass of the vaporized species.

It can easily be seen that maximum rate appears when p=0 and C=1. The actual evaporation rate will be $\frac{1}{3}$ to $\frac{1}{10}$ of the maximum rate. This because there will, among other factors, be surface contamination and collisions within the vapor.

The flow of the evaporated material from the source towards the substrate would, without any collisions, go in a straight line (e.g., line-of-site deposition). Based on a point source material the distribution of deposited material will be followed by a cosine distribution in Eq (3.2).

$$dm/dA = (E/\pi r^2) cos\phi cos\theta \tag{3.2}$$

where dm/dA is the mass per unit area, E=the total mass evaporated, r=the distance from source to the substrate, θ = the angle from the normal to the vaporizing surface and ϕ = the angle from the source to the substrate line

Depending on the vapor pressure of the material being evaporated the deposition rate can vary. The equilibrium vapor pressure is defined as the vapor pressure of the material in equilibrium with the solid or liquid surface in a closed container. At equilibrium the same amount of material are leaving the surface as are returning to the surface. The materials vapor pressure decide whether there will be a useful deposition rate or not. If the vapor pressure to the material is 10^{-2} Torr above the solid the material is described as a subliming material. If the vapor pressure is 10^{-2} above the liquid melt the material is described melting. A problem with subliming materials are the poor contact to the resistive heater. Some subliming material, like Cr, also need a slowly heating process so alloys like H can out gas before pure chromium is evaporated.

For vaporization to take place the surface and a large volume of material must be heated to an appreciable vapor pressure. The most common way for materials evaporating beneath 1500 ^{o}C is by resistive heating where a current is running by a material where the material is in contact. The voltage used is often little (<10V), but a large current (>several hundreds ampere) are sent through hairpin, spiral, boat, basket or a crucible. It depends on the material what the heater is. Typically materials for the heater are W, Ta, Mo, C and BN/TiB_2 composite ceramics.

A vacuum chamber for deposition is usually quite large. That gives a long

distance from the source to the substrate to avoid radiation from the source to the substrate. A shutter is placed between the source and the substrate so the evaporation can stabilize before the deposition takes place. The shutter must be placed in such a way that the source does not have "eye-contact" with the substrate. If a crystal monitor is used the source should have "eye-contact" all the time so the rate can be followed easily.

Sometimes it is useful to heat up the substrate before depositing. To get high quality samples through PVD with a resistive heater, monitoring is needed. This can be done by having a resistive heater above the substrate and heat it up by radiation. If a cool substrate is wanted the most convenient way to cool it down is by water cooling.

In a chamber it is usual to have chamber pressure-, temperature-, deposition- and vaporization-source monitors. Not all of the monitors are needed to make good films, but a deposition monitor is the least you need. This monitor often uses a quartz crystal monitor that is piezoelectric. That means that an AC voltage causes a movement which resonates with a frequency dependent on the thickness of the crystal and its orientation. By calibrating the monitor due to the density of the evaporating material the rate can be decided by measuring the change in the resonance frequency.

To get the best samples possible we want to avoid contamination. Contamination can come from the deposition system, the substrate or the source of film material.

Vacuum deposition has several advantages, among them are:

- deposition rate monitoring is relatively easy
- high deposition rate can be achieved
- source material is relatively inexpensive
- the technique is relatively inexpensive compared to other PVD techniques

Also disadvantages follows, such as:

- poor utilization of vaporized material

- line-of-sight deposition gives poor surface coverage and does not deposit uniformly
- high radiant loss during processing
- few processing variables for film property control

A conclusion of vacuum deposition as a PVD can therefore be said as a energy efficient process which is relatively simple and inexpensive, but can cause some problem if a very uniformly deposition is needed.

3.2 Characterization methods

3.2.1 Stylus Profilometer

The section is based on chapter 3 in [32]

A stylus profilometer is a contact method of measuring the height of a thin film. A stylus is pressed towards the sample while either the stylus or the sample is moving. When scanning the surface the stylus converts its movement into electrical signals depending if the stylus is pushed up by the film or down in a cavity of the film. The signal is then amplified and is given out as topological graph over the surface of the film.

To get a good graph over the profiled surface the surface must be free for contamination. Dust will appear as bumps on the scanned surface. The lateral accuracy of a profilometer is strongly dependent on the stylus radius. A sharp edge or a vertical step in the sample will look like a round edge in the graph. A long high vertical step will show a cone angle slope.

The surface measurement depends on the roughness of the sample, the instrument's electronic noise level, the mechanical stability of the stylus and the signal's height digitization increment. The surface profiles can therefore be different from profilometer to profilometer, and also within the same profilometer. To average, and that way gain reliability of the measurements, the surface can be scanned several times and the scans can be averaged or compared.

In this thesis the thicknesses of the samples were measured with a α step 100 profilometer. The films investigated were on transparent substrates as microscope slides, fused silica and sapphire. The measurements were done at Professor Ursula Gibson's lab at NTNU.

3.2.2 UV-Visible-NIR spectrophotometry

To create an absorption, transmission or intensity spectrum spectrophotometers are common used. A source sends lights consisting of a broad band of light, typically 200nm up to 800nm towards a sample and a detector, the spectrophotometer. At some wavelengths the intensity of the incident ray will transmit through the sample, but at other wavelengths the intensity will be absorbed. The intensity of the transmitted ray depend on the incoming intensity, the absorption coefficient and the thickness of the sample. The transmitted intensity can be found by Eq (3.3)

$$I = I_0 e^{-\alpha t} \tag{3.3}$$

where I_0 is the intensity to the incident ray at a given wavelength, I is the transmitted intensity, α the absorption coefficient and t the thickness of the sample. The transmission is given as

$$T = \frac{I}{I_0} \tag{3.4}$$

From Eq (3.3) and Eq (3.4) the absorption coefficient of a sample can be estimated. This is given in Eq (3.5).

$$\alpha = \frac{1}{t} ln(\frac{1}{T}) \tag{3.5}$$

The characterization method with a spectrophotometer differs whether the spectrophotometer uses a single beam or double beam. When measuring with a single beam, I_0 is found from a reference made from a clean substrate. For a double beam the reference intensity is made simultaneously as the sample is measured. This way I_0 is the intensity in air, and not through the substrate.

The absorption is seen as tops in the absorption spectrum and drops in the transmission spectrum. This can be used to characterize the band gap of the material, the photoluminescence and the excitation of electrons.

To measure the transmission spectra in UV-VIS two spectrophotometers were used. All the samples on the transparent substrates were measured. The source was a Mini-D2T from Ocean Optic, Inc and the detectors were a CCS100 from ThorLabs and an AvaSpec from Avantes. The range was from 322-740 nm and 250-1000 nm respectively. The measurements were performed at Ursula Gibson's lab at NTNU.

The absorption spectrum from 200nm to 3000nm is made for three samples. One contained 31% Cr and the two others should contain 5% Cr. The performance was done by Irina T. Sorokina in a CAREY 5 spectrophotometer at the University of Vienna.

To see the effect of samples deposited on hot substrate a diffuse reflectance spectrophotometer is used. For this case it was a Perkin Elmer Lambda 650 spectrophotometer measuring in the range from 1200 - 2500 nm. The spectroscopy was taken on the samples made on the "wrong" side of Si wafers. The measurements were performed at the Department of Chemistry at NTNU.

3.2.3 Fourier-Transform InfraRed spectrophotometry

FTIR spectroscopy is a technique for measuring absorption, transmission or reflectance depending on the choice of beam splitter, source and detector in the NIR-IR area. FTIR can measure over a wide spectral range, typically 0,7 μm - 500 μm, and properties of both gas, liquid or solid. Since FTIR uses the up-set of a Michelson's interferometer a broad range of wavelengths can be measured simultaneously. This gives FTIR a huge advantage over the dispersive spectroscopy which only can measure a narrow range at the one time and then need to re-do the measurement for the next wavelength[33].

To be able to measure the wide spectrum of wavelength simultaneously a IR beam, consisting of a wide range of wavelength, is sent towards a beam splitter. This splits the beam and send 50% towards a fixed mirror and 50% towards a moving mirror. The beams are then reflected by the mirrors and sent back towards the beam splitter, which is the basic behind the Michelsons interferometer. Now, only beams of constructive interferrence can let through

the beam splitter and sent towards the sample, where the absorption occur, before the beam reaches the detector. Since the FTIR makes an interferogram this has to be converted to a spectrum. This is done by Fourier Transform of the signal.

A Tensor 27 FTIR spectrophotometer was used to determine the spectrum from 2500 nm to 25000 nm for some transparent samples. The measurements took place at Professor Ursula Gibson's lab at NTNU.

3.2.4 X-ray Diffraction

XRD is a method used to determine the atomic structure, lattice constant and Debye-Waller factors of a ordered crystal in three dimensions. Through XRD the crystal formation, roughness, kinetic aspects and thermodynamic can be probed. The accuracy of an XRD in determine lattice parameter is in the order of 0.01 Å [34].

In an XRD X-rays are sent towards the sample and a detector from an X-ray generator. During measurements the sample will change an angle Θ while the detector moves 2Θ. At certain angles constructive interference appear for the structure planes in the thin films and the substrate, if the substrate has a lattice configuration. By knowing the diffraction angles for the thin film it's lattice configuration can be found. Figure (3.1) gives an illustration of an XRD up-set.

XRD was used to determine the affect of annealing of the samples and to see if films deposited at room temperature had a lattice structure. A sample with pure ZnS was examined in a 2θ spectrum from 20-70 degrees before and after annealing. This also counts for samples containing 31%, 7% and 12% Cr. Sample of ZnS:Cr deposited on hot sapphire substrate with a theoretically concentration of 4% was also examinated. The measurements were done in a D8Discover at the Department of Electronics and Telecommunications at NTNU .

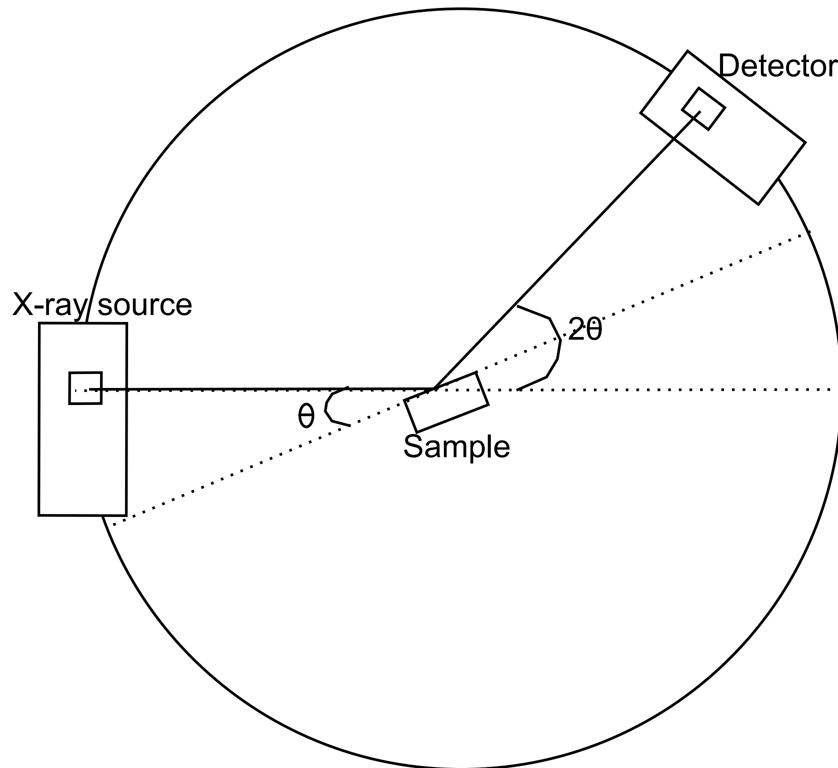

Figure 3.1: *The principles behind an XRD system. The source is fixed, while the sample holder and detector are moving. As the sample moves an angle θ, the detector moves 2θ. When X-rays collide with electrons in the lattice a diffraction pattern can be revealed.*

3.2.5 Auger electron spectroscopy

Sending an electron beam with a certain energy towards a sample, electrons can encounter or collide with an atom in the sample. How far the electrons will penetrate is dependent on the energy of the beam. However, the penetration depth fall off for specimen at high atomic number because there are more particles to stop the penetration from the electrons. When the sample is hit by electrons with low energy it will cause an ionization of an atom in an inner shell. This makes an atom from a outer shell to fall in to fill the free vacancy, releasing excess energy. If this energy coincides with an electron in an outer shell the atom will release this electron which is known as an Auger electron. Auger electrons can only be emitted from the near surface because of its low energy, often just a few nm or atomic layer into the sample. Because of the released excess energy coincides with one particular electron

energy and it's binding energy, chemical composition from the sample can easily be found. AES is therefore mostly used in surface analysis [35, ch. 1].

Four samples were investigated in the Auger. A 3690 Å thick 7% sample, an 800 Å thick sample with less than 5%, a 270 Å thick sample with 31% and a sample which was deposited on hot substrate. This sample should contain 80 Å Cr from the quartz monitor, which would make the Cr concentration 4%.

The measurements were done in a JAMP-9500F Field Emission Auger Microprobe at the Department of Electronics and Telecommunications at NTNU.

3.2.6 Hall measurement

Hall measurement is a way of characterizing the carrier density and type of carriers, e.g. electrons or holes and give an I-V curve. The principle can be easily explained by considering the Fig. (3.2). A sample with four connectors is placed in a magnetic field. A current is flowing between C and D. The carriers experience a Lorentz force and concentration builds up to form a field to balance the Lorentz force. To maintain a steady flow of carriers through the sample an electric field has to be established to counteract the induced field. This is known as the *Hall-effect*. The field times the width of the sample is known as the *Hall-voltage*. Depending if the carriers are holes or electrons the voltage will be positive or negative. The voltage can be measured and both the doping concentration, e.g. number of carriers, and the doping type, e.g. n-doped or p-doped, can be estimated [10].

The doping level and the carrier distribution of sample 3 and 4 containing 30% and 10% Cr respectively were calculated during Hall-measurement at the Department of Electronics and Telecommunications. The instrument used was a Lakeshore Model 7504.

3.2.7 Four probe measurement

Four probe measurement is a way of measure the resistivity of a material. The setup is shown in Fig. (3.3). An electric voltage is applied and a current is sent through the sample through the outa two of the contacts. The other

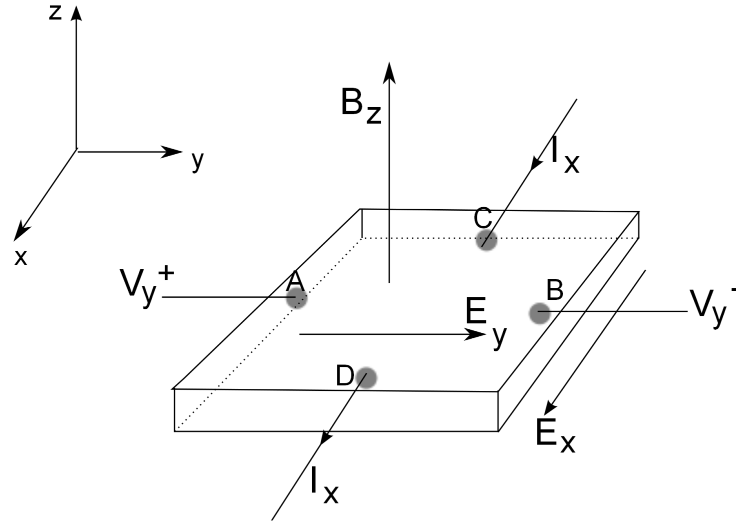

Figure 3.2: *Schematic description of how the Hall-measurement. A sample is placed in a magnetic field in the B_z direction and a current is sent in the I_x direction. This induce an electric field, the Hall-effect, between A and B, marked E_y.*

are used for measuring the voltage which is caused by the external voltage. The resistivity per area of a material on an insulating substrate is found by Eq (3.6) [36].

$$\rho = \frac{\pi d}{ln 2 I} = 4.53 \times \frac{V}{I} d \tag{3.6}$$

The resistivity of the all the samples were found at a four-probe set-up at Professor Ursula Gibson's lab at NTNU in a Signatone S-301-4. The probes were placed after each other in a row. A 1kΩ resistance was connected in series to lower the current in the circuit.

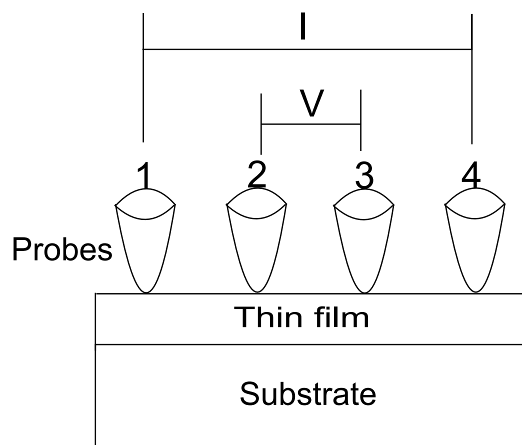

Figure 3.3: *Schematic description of a Four probe measurement. A probe with four contacts is pushed down on the sample. A current is applied between two of the probes when the to others measuring the voltage between the two others.*

3.3 Preparation methods

3.3.1 Building the lab

The first 4 weeks of this semester the lab had to be built. Since the system came from USA the plugs and fuses had to be converted from 110 V to 220 V. The deposition system used a mechanical pump and a diffusion pump to purge down to vacuum. The heater in the diffusion pump was substituted and all the plugs were changed. The fuses and plugs for the monitors were also substituted. Some of the wires were old and were changed. The mechanical pump were built in a box surrounded by acoustic tiles and couplet up to an outlet. This way the oil exhaust did not pollute the lab with oil mist. Also the water hoses and the hose nipples used for cooling of the diffusion pump were changed. As ZnS and Cr should be deposited simultaneously a partition wall was made and attached to the system so the crystal monitors only could see one source.

3.3.2 Sample preparation

Three different substrate were used for deposition. These were microscope glass, fused silica e.g. SiO_2 and sapphire e.g. Al_2O_3. All three substrates are transparent and insulating oxides with good transmission in low UV. Their infrared transparency varies. Both the fused silica and the microscope glass shows transparency between 250 nm up to 4 microns, though the fused silica has an absorption line at 2.7 microns. The sapphire shows transparency up to 7 microns and is therefore a suitable substrate for this purpose.

Samples in size of 0.25" X 0.25" are made from 1" X 1" glass. The pieces are put in a a solution of alconox powder and hot water and then in ultrasonic bath. The samples are then rinsed in running water. Then they are put in acetone for ultrasonic bath. The procedure is repeated with isopropanol. The ultrasonic bath last for 9 minutes for all cases. Just before the samples are put into the chamber they are dried with nitrogen, N_2. The substrate is then put into the chamber.

3.3.3 Deposition

For the sample preparation in this work PVD with resistive heating was used. A sketch of the system is shown in Fig. (3.4), and pictures are given in Appendix C. The chamber is pumped down using a mechanical pump and a diffusion pump. The base pressure selected is 6-7 $*10^{-6}$ Torr. The distance between the sources and the substrate is 30 cm and approximately 20 cm to the crystal monitors.

During deposition the substrates are exposed for a ZnS source and Cr source at the same time with different rates. The difference in sample rate of each source determine the thickness and the relative amount of Cr in the samples. A piece of stainless steel making a partition wall is placed between the two sources to prevent cross-talk between each source and the monitor for the other material. This way each monitor is used for just one source and the amount of each material can easily be followed.

For the Cr source a Cr-coated refractory metal is used. For depositing ZnS a Mo-boat is used. Since ZnS is a transparent medium the thickness does not affect the properties in the same way that Cr does. The thickness of ZnS can

therefore variate depending of the concentration of Cr in the sample. Cr is not transparent, so the thicknesses of Cr are selected to stay beyond 50 Å.

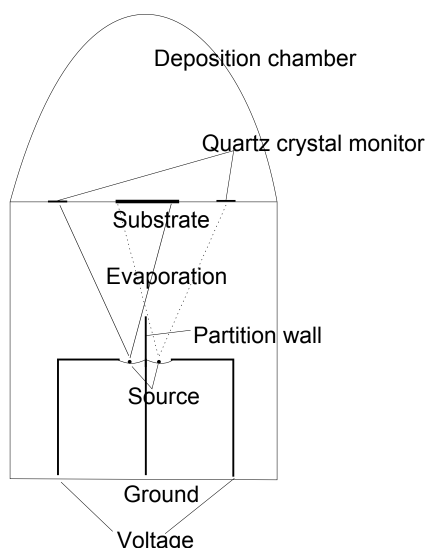

Figure 3.4: *Schematic description of the deposition chamber. To source are divided by a partition wall. The substrate is placed above the sources. Next to the substrate two quartz crystal monitors measure the rate for each of the sources.*

The Cr rod could not handle very large current and high rates, since it easily broke during test depositions. The rate was therefore limited to between 0.2 and 0.6 Å/s. The deposition time was around 2 minutes. Depending on the amount of Cr desired in the sample, the rate of ZnS varied. A very thick sample with 1% Cr was also made. The rate of Cr for this sample was 0.1 Å/s and the rate of ZnS was 10 Å/s for. The deposition time was 10 minutes.

Several samples were also made at the same time. Samples are put simultaneously in a sample holder, but at different places and distances from the two sources. This way the effect from the position of the substrates can be detected and multiple concentration levels could be deposited in one run.

Deposition on hot substrates has also been performed, both on sapphire substrate and the rough side of Si wafers. The temperature of the substrate was selected to be 300^0. The temperature was measured with a K-type thermocouple coupled to a multimeter measuring the voltage. The voltage was converted through a data sheet for K-type thermocouples before a converter

was found.

Even though there is one crystal monitor monitoring each source it important to re-examine the samples to see how big the amount of Cr is. Most of the substrates are therefore dressed with aluminum foil on one edge facing towards one source, e.g the Cr during deposition. Only the Cr will go beneath the aluminum foil. Looking in a profilometer you can measure the height of Cr and the total height on the rest of the sample. By subtracting Cr from the total hight of the sample the height of ZnS can be found and also an estimate if the sample has the amount of Cr that was predicted.

After the samples were made they were investigated in the UV-VIS-NIR spectrum and by four-probe measurement. Hall-measurements, annealing, XRD and AES were performed on a selection of the samples.

Chapter 4

Results and Discussion

In this chapter the results from the performed measurements will be presented. I will also discuss the results based on theory and the experimental work. The chapter starts with the deposition facts of the samples. The results from the profilometer is followed by a short discussion of the predicted concentration, and the actual thickness. Then the spectra in UV-VIS and NIR are presented. From the spectra a discussion is presented an also an estimation of the band gaps for the samples is given.

Based on the results from the XRD and the AES spectroscopy the chemical compositions of some of the samples will be discussed. A discussion of the effect annealing and deposition on hot substrate played will also be given. At the end I give the results from the Hall-measurements and the four-probe measurements and discuss the results shortly.

It must been said that spectrophotometers in the wanted range was difficult to obtain until the end of the term. This counts for the NIR spectrophotometer between 1200-2500nm. There also seemed to be an artifact with the spectrophotometer in the visible range, since it gave periodic bumps in the spectra. A new spectrophotometer was therefore tried. The absorption coefficient and the Tauc plot are based on samples measured in the spectrophotometer with the artifact, however, the artifact will probably not affect these plots since the bumps occur periodically and at same wavelengths for all samples. Four samples are investigated in the spectrophotometer without the artifact, one of them is the same sample before and after annealing. The results is then compared to the old results in the old spectrophotometer.

4.1 Deposition parameters and thickness measurement

Several samples are made, both on sapphire, quartz, the backside of a Si wafer and on microscope slides. The concentration varies between 30% to 4% from the crystal monitors, and 32% to 7% based on measurements examined in the profilometer. Also the thicknesses of ZnS and Cr were varied to adjust the optical spectra. The deposition parameters and the thickness measurements are shown in Table 4.1. Fucluded are the deposition rate, concentration and thickness from the crystal monitors. Also the thicknesses estimated from the profilometer are given.

During deposition, quartz monitors were used to control the deposition rate and thicknesses of ZnS and Cr, and thus the concentration of Cr in the samples. However, for some samples the thicknesses of Cr and ZnS showed rather big differences in the thicknesses measured by the monitors. All the samples except sample 16-20 were partially covered with aluminum foil. This way both the Cr and the total thicknesses could be re-examinated in a profilometer.

Sample 6, 7 and 8 were deposited at the same time. Sample 6 was closest to the Cr source, sample 7 was centered between the Cr and ZnS source, while sample 8 was closest to the ZnS source. Sample 10-15 were also deposited simultaneously. Here sample 14 was centered between the two sources. Sample 10, 12 and 13 were closest to the Cr source while sample 11 and 15 were nearest the ZnS source. Due to the low concentration, the profilometer only gave results for the Cr concentration for sample 10. For sample 11-15 the roughnesses at the surface made it difficult to determine the thickness of the Cr layer and only the total thicknesses were found. The samples made on Si could not be examined in the profilometer because of the roughness of the substrate, even though the quartz monitors registered 1200 Å.

The measurements have an accuracy around ±25 Å. This leads to an uncertainty of the measurements from the profilometer of several percent. The temperature of the substrate for heated deposition was 300° C. Annealing in sealed quartz ampules was performed at 450° C for two hours.

Table 4.1: *The data from the monitors during deposition and the profilometer after the deposition. As can be seen there is a deviation for the wanted deposition concentration and the post-examination. For the samples were the concentration could not be estimated from the profilometer an x is denoting the concentration.*

No:	**Target conc.**	**Meas. conc.**	**Substrate**	**Meas. thickness**	**Rate ZnS**	**Rate Cr**
1	4%	x	Microscope glass	310 Å	4.5 Å/s	0.2
2	32%	21%	Microscope glass	2052 Å	4.1 Å/s	1.2 Å/s
3	22%	31%	Sapphire	370 Å	1.8 Å/s	0.5 Å/s
4	10%	12%	Sapphire	542 Å	3.8 Å/s	0.4 Å/s
5	5%	7%	Sapphire	3340 Å	2.9 Å/s	0.2 Å/s
6	11%	15%	Silica	500 Å	3.8 Å/s	0.4 Å/s
7	11%	11%	Sapphire	540 Å	3.8 Å/s	0.4 Å/s
8	11%	8%	Silica	570 Å	3.8 Å/s	0.4 Å/s
9	5%	x	Sapphire	300 Å	3.8 Å/s	0.2 Å/s
10	5%	20%	Silica	750 Å	3.8 Å/s	0.2 Å/s
11	5%	x	Sapphire	800 Å	3.8 Å/s	0.2 Å/s
12	5%	x	Silica	200 Å	3.8 Å/s	0.2 Å/s
13	5%	x	Silica	350 Å	3.8 Å/s	0.2 Å/s
14	5%	x	Sapphire	400 Å	3.8 Å/s	0.2 Å/s
15	5%	x	Sapphire	545 Å	3.8 Å/s	0.2 Å/s
16	8%	x	Sapphire (300^0)	270 Å	4 Å/s	0.2 Å/s
17	4%	x	Sapphire (300^0)	830 Å	5.6 Å/s	0.3 Å/s
18	14%	x	Si (300^0)	x	7.0 Å/s	1.2
19	14%	x	Si	x	7.0	1.2
20	14%	x	Si	x	7.0	1.2
21	0%	x	Si	x	5.0	x
22	0%	x	Silica	1230 Å	3.8 Å/s	x

Some samples show big differences between the measured thickness and the intended thickness from the monitor. There exists several reasons for this. One fact is that when ZnS evaporates, surface mobility of the arising molecules is very large, and significant re-evaporation can occur [37]. This

counts especially for the heated substrates. Another fact is that during deposition the monitor measuring the Cr rate was affected by the ZnS source. Because of the long time needed to heat up Cr [31], the Cr source was turned on before the ZnS source, and was stabilized. Despite the shield between the sources, the Cr rate during deposition increased when the ZnS started to evaporate.

The distance between the substrate position and the crystal monitors most likely also played an important role in the thickness deviations of Cr and ZnS in the sample. The monitors were placed below the shutter so the stabilization of the sources could be observed before the shutter was opened. The distance between the monitors and the sample was 10 cm. The monitors were also placed in a horizontal distance from the side of the substrate.

One reason why sample 10 and 11 show big deviation from the rate monitor, can be a result of the shutter was too small to cover all samples simultaneously. The measured deposition time and rate can therefore be incorrect. However, the position of the substrates relative to the source centers is strongly related to the deposited thickness. This is observed from the films made simultaneously. A lateral shift of one cm leads to a large difference in the sample thickness. Even though the source is not a point source the relation between the lateral shift and the thickness can be understood by Eq. (3.2) which shows that the evaporation from a point source occur in a cosine function. Changes in alignment can occur during sample loading and during replacement of the Cr rod and the Mo-boat. This will lead to varying conditions for the deposition. Also the fact that the distance between the crystal monitors and the source is less than the source-substrate distance can play a role.

For the case of the hot-substrate depositions, two samples were made on sapphire. Sample 16 was only investigated in the profilometer where it was found that only 270 Å of deposited material adhere to the substrate even though 520 Å was deposited. A new sample was therefore made by depositing 2074 Å where 80 Å was Cr. However, measurements from the profilometer showed a thickness of 830 Å. Aluminum foil was not used during deposition onto the heated substrate, mainly because of the damage the hot substrate could do to the foil. The difference between the film thickness on the substrate and the monitors can be due the fact that the monitors are not heated to the same temperature. This can affect the monitors and thus show a higher rate than what is actually deposited onto the sample, or re-evaporation as observed on [37]. The thermocouple was not calibrated, so the temperature

can have been higher than 300^0 C. Subbaiah et.al. reported of amorphous structure for substrates deposited above 350^0 [27].

Sample 18, 19 and 20 were deposited simultaneously. Sample 18 and 19 in room temperature while sample 20 was deposited at 300^0 C. For sample 18 and 19 the film looked blue, but the film on sample 20 could not be seen with the eyes. There was a separator of approximately 1 cm between each of the three samples. The samples could not be investigated in the profilometer because of the roughness of the substrate.

The thicknesses and concentration for the thin film profiles also vary several percentage within the same sample. For the low concentration samples it was not possible to measure the height of the Cr because of the accuracy limitation for the profilometer.

4.2 Transmission spectra

The samples are measured in five spectrophotometers. All samples except 18, 19 and 20 are measured in the visible range from 322 nm up to 740 nm. Sample 18-20 were measured in a spectrophotometer using diffuse reflectance in the range 1200 nm to 2500 nm. Sample 3, 11 and 15 were also measured in a wide spectrum from 1500 nm to 3000 nm. A selection of samples were also investigated in the FTIR from 2500-25 000 nm. After it was concluded that the spectrophotometer had an artifact, sample 4, 5, 17, 22 and both the not-annealed and the annealed part of sample 3 were re-measured from 250-1000 nm.

UV-VIS

Before the measurement started the spectrophotometer was calibrated with a He light.

A plot of sample 22 deposited on fused silica and a model of a 900 Å thick ZnS film is shown in Fig. (4.1). As can be seen, both increases at low wavelength due to interference fringes. This coincide also well for other low doped samples. The ZnS thin film has an abrupt fall towards the band edge at 336

nm which corresponds to 3.68 eV. This coincide to previous results for cubic structure [30]. The modeled ZnS film do not follow the fall towards the band edge. This is because the model only consider the interference which occur within the film, and not the absorption at low wavelengths.

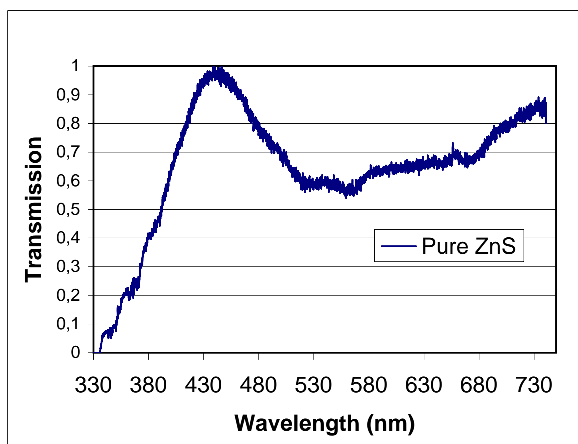

(a)

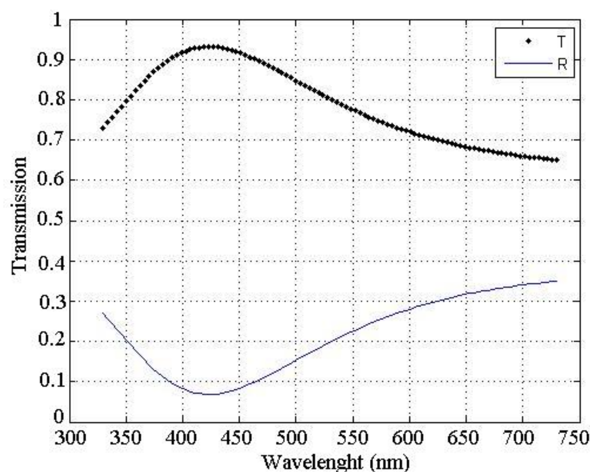

(b)

Figure 4.1: *Shows the transmission spectrum for a model made from 900Å thick ZnS on quarts. In (b) the measured spectrum is showed as a function of wavelength through a 1000 Å thick ZnS film made on SiO_2 substrate. The increase in transmission at lower wavelength is due due to interference in the film.*

The transmission spectra for the sapphire samples in visible spectra are shown in Fig. (4.2) and Fig. (4.3). The spectra show multiple peaks. This was first thought of as interference effects. The peaks continue almost periodic through the spectra. However, based on previous work no absorption should occur in this region for low levels of Cr [17].

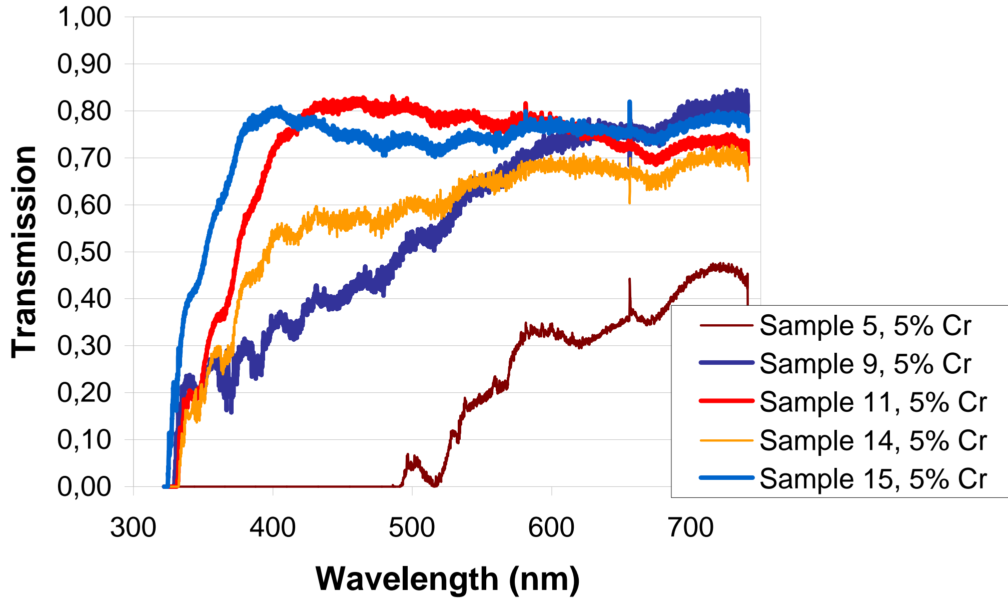

Figure 4.2: *Transmission spectra for sample 5, 9, 11, 14 and 15 deposited on sapphire as a function of wavelengths.*

Samples 9, 11, 14 and 15 are made at the same time on sapphire substrate, but with a graded Cr amount. The sample closest to the ZnS source, e.g. sample 11 and 15, show highest transmission in the low wavelengths before the abrupt fall towards the band gap. This sample does not contain more than maximum 5% Cr. Sample 9 and 14, which were made during the same deposition, were closest to the Cr source and is meant to have higher concentration of Cr. These samples show a much lower transmission spectrum at low wavelengths. This imply a more insulated and non-transparent film. However, the abrubt fall at the band edge seems to coinside for all of the samples, both high and low concentration of Cr, and at wavelengths above 600 nm they show approximately the same transmission as the lower doped samples. The low concentrated samples can be compared to the spectrum

for sample 22 showed in Fig. (4.1). As can be seen, the graphs with small amounts of Cr and ZnS have the same shape throughout the spectrum. The band gaps seem also to coincide with the pure ZnS sample. This may imply that the sample does not contain Cr or the concentration is very low.

Sample 3, 4 and 7, containing 31%, 12% and 11% Cr respectively, measured from the profilometer, are shown in Fig. (4.3). Sample 7 was deposited simultaniosly as sample 6 and 8, but centered between those two. However, the sample shows the same curvature as less doped samples, and a big deviation compared to sample 4 which has the same concentration of Cr. The thickness is also approximately the same as for sample 4. However, sample 4 looks more metallic than sample 7. It is believed that sample 7 contains less Cr, or sample 4 more, than what is estimated from the profilometer.

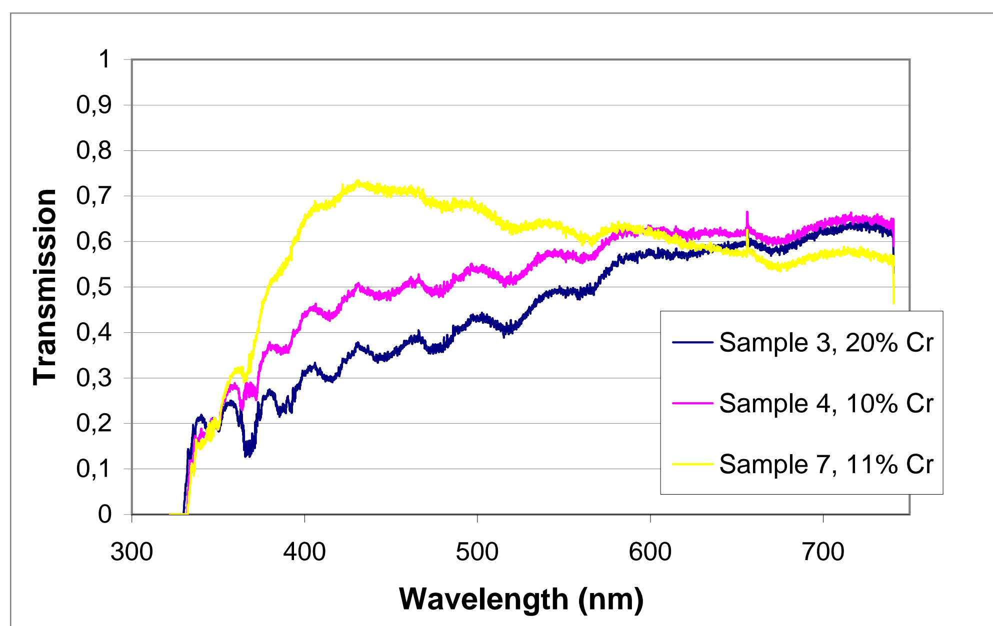

Figure 4.3: *Transmission spectra for sample 3, 4 and 7 deposited on sapphire as a function of wavelengths.*

The samples made on fused silica are shown in Fig. (4.4). Sample 10, 12 and 13 were made during the same deposition as 9, 11, 14 and 15.

As can be seen from Fig.(4.4) samples with low concentration of Cr coincide with the ZnS spectrum, Fig. (4.1), and those interference fringes that appears

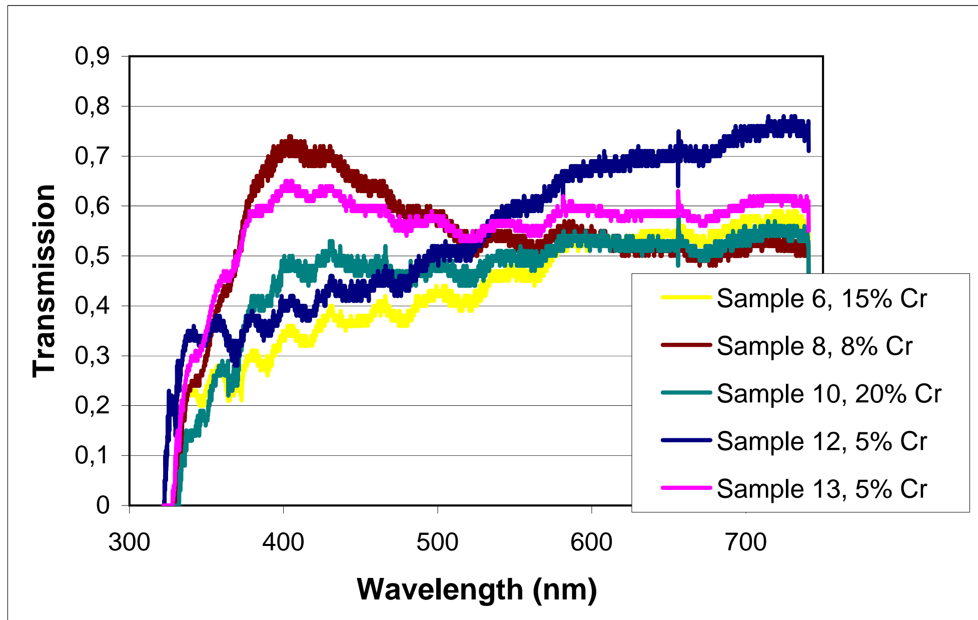

Figure 4.4: *Transmission spectra for sample 6, 8, 10, 12, 13 deposited on fused silica as a function of wavelengths.*

in pure ZnS. The spectrum for the higher doped samples fall off toward lower wavelengths and have an abrupt cut-off around 330 nm, corresponds to 3.75 eV. The fringes that was thought of as interference fringes, also appear for the samples that were made on fused silica. Even though there has been reported of birefringes in fused silica [38][39], some samples were investigated in another spectrophotometer.

As mentioned, the first idea of what caused the bumps in the spectrum were interference fringes which occur in the substrate since sapphire is a birefringence material. Also fused silica has been shown to have birefringe effect [39]. Interference can also occur in the thin films itself [40]. The films were also made on sapphire that was randomly cut, which could give an interaction between the light and the substrate, or the light source could be polarized. However, after seeing the same fringes on samples made on microscope slides, and the fact that the fringes appear periodic, the idea of an artifact in the spectrophotometer causing the periodic waves appeared. Another spectrophotometer was therefore tried.

The new spectrophotometer was calibrated with a He light source. The He spectrum from the spectrophotometer and spectrum which it is compared with, are shown in Fig. (4.5). The new measurement of sample 3, 4, 5 and 17 are given in Fig. (4.7), Fig. (4.8), Fig. (4.9), and Fig. (4.10) respectively.

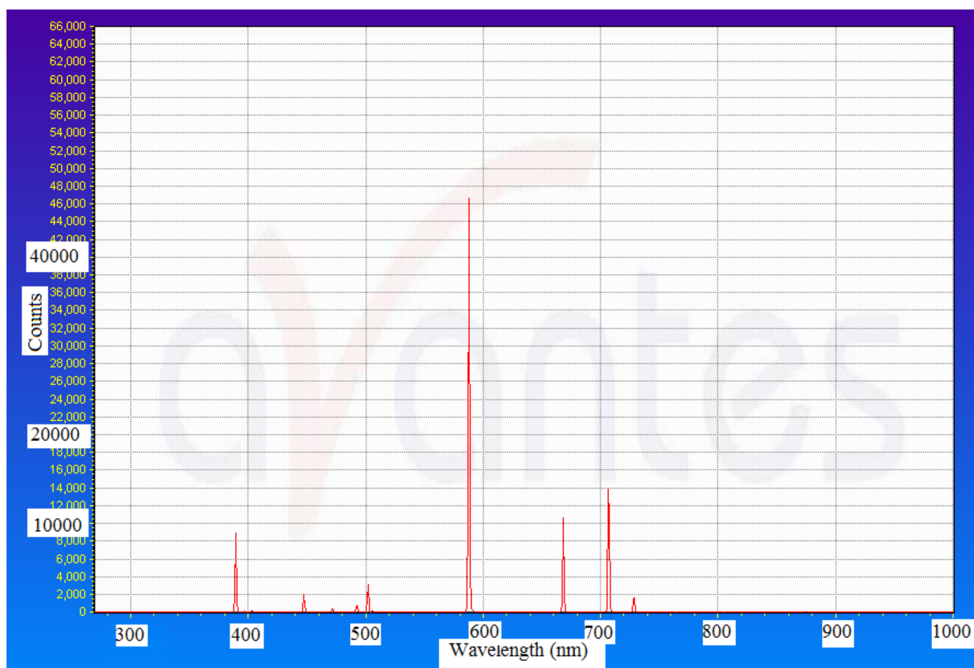

(a)

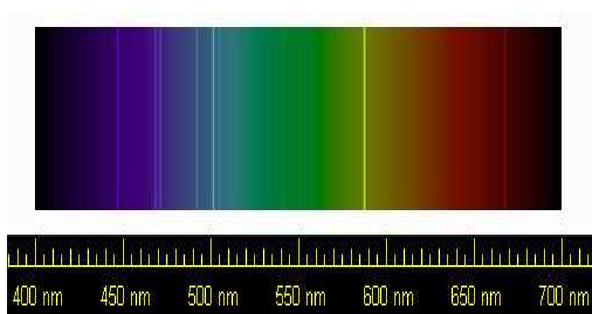

(b)

Figure 4.5: *(a), the He-spectrum from the spectrophotometer. (b), a specter of where He-lines shall occur. Figure (b) taken from* [41]

As can be seen from Fig. (4.7(a)) and Fig. (4.7(b)) the annealing effect did not affect the optical measurement in the UV-VIS spectrum for sample 3. Both sample have scars and scratches after being measured. This can cause

the transmission in the lower wavelength area. It can also indicate that the sample is most likely comprised of clusters in a dielectric matrix. This makes the film more insulating [42], and further an increase in the band gap which can be the reason why the abrupt fall towards the band edge is absent. The fact that the old spectrophotometer had low intensity at low wavelength can also lead to the abrupt fall in transmission in Fig. (4.3), but for the spectrophotometer with a higher intensity the transmission through the sample was highly increased. The annealed sample did also crack during the annealing process. This also occurred for sample 22 during annealing. A picture of sample 22 before and after annealing is shown in Fig. (4.6). This can happen because of the tensile stress in amorphous films caused by the high temperature and slow cooling as reported in [43]. A picture of the transmission spectrum before and after annealing is shown in Fig. (4.7).

Figure (4.8) and Fig. (4.9) show transmission spectra from the new spectrophotometer for sample 4 and 5 respectively. Sample 4 shows an abrupt change in the transmittance at 390 nm, but it has a tail which flattens out at 320 nm. This can be because the sample has scratches and defects that let light through below 320 nm, or that Cr clusters make the film insulating [42]. By extrapolate the abrupt change the intersection at the x-axis is estimated to 4.4 eV. This is an highly increase of the band gap compared to pure ZnS. It is therefore reasonable to believe that also this sample contains Cr cluster.

In the old spectrophotometer sample 5 seemed to be too thick, and too little transparent, to give an reliable estimate of the band gap. However, in this spectrophotometer interference fringes appear, most likely because of the film thickness, but also an abrupt fall in the transparency at 560 nm. By extrapolating the abrupt change in the curve, the band gap is estimated to be 2.95 eV. This is lower than for pure ZnS, which may imply that Cr has interacted with ZnS, making free carriers of Cr and making the band gap smaller.

Sample 17, Fig. (4.10), also shows a tail for short wavelengths. The fringe probably appear as a result of the thick film on the substrate. It coincide well to Fig. (4.1(a)), which implies a low, or none, concentration of Cr. By extrapolating the abrupt change in the spectrum the band gap is estimated to 310 nm, which corresponds to 4 eV. This imply Cr clusters making the film more insulating than pure ZnS.

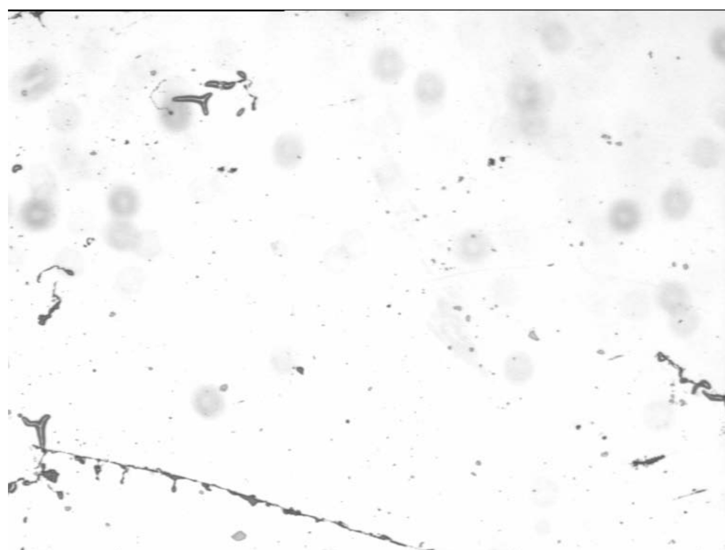

(a)

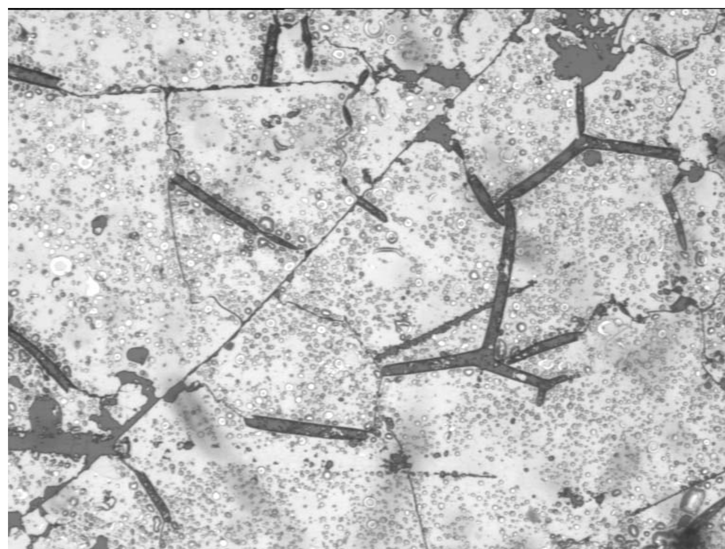

(b)

Figure 4.6: *The ZnS film on fused silica before annealing in (a). No big cracks are observed. In (b) the same sample is shown after annealing. Several big cracks can be observed.*

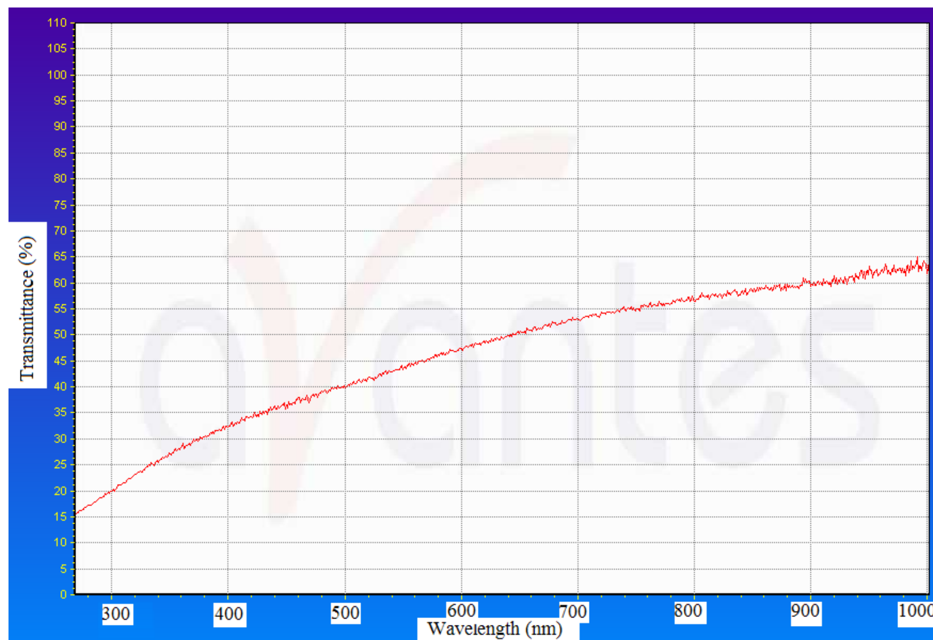

(a)

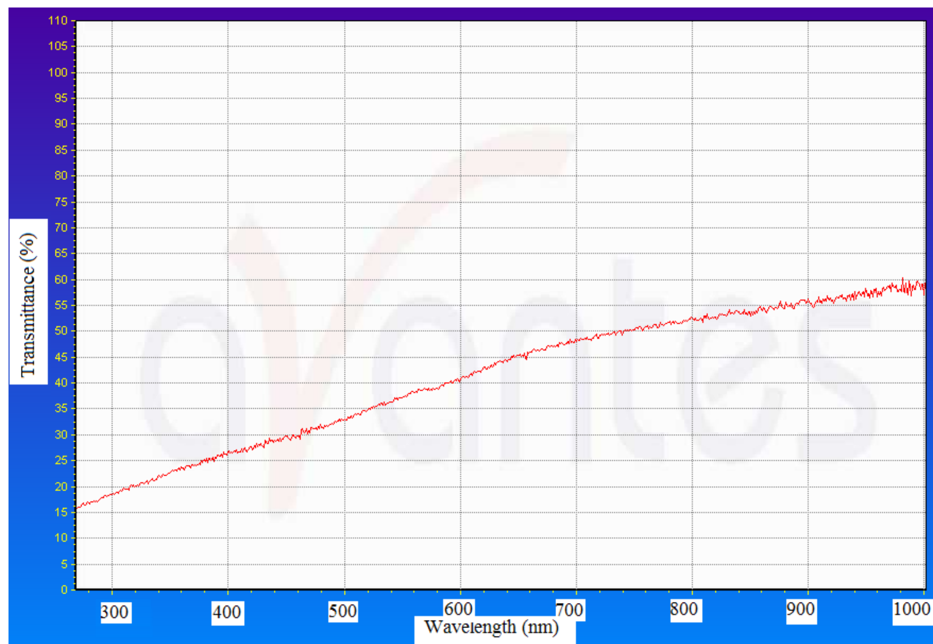

(b)

Figure 4.7: *The transmission spectra for sample 3. (a) shows the non-annealed sample of 31% Cr and (b) the same sample after annealing. There is no big deviations from the figures, and both seems insulating with a high band gap.*

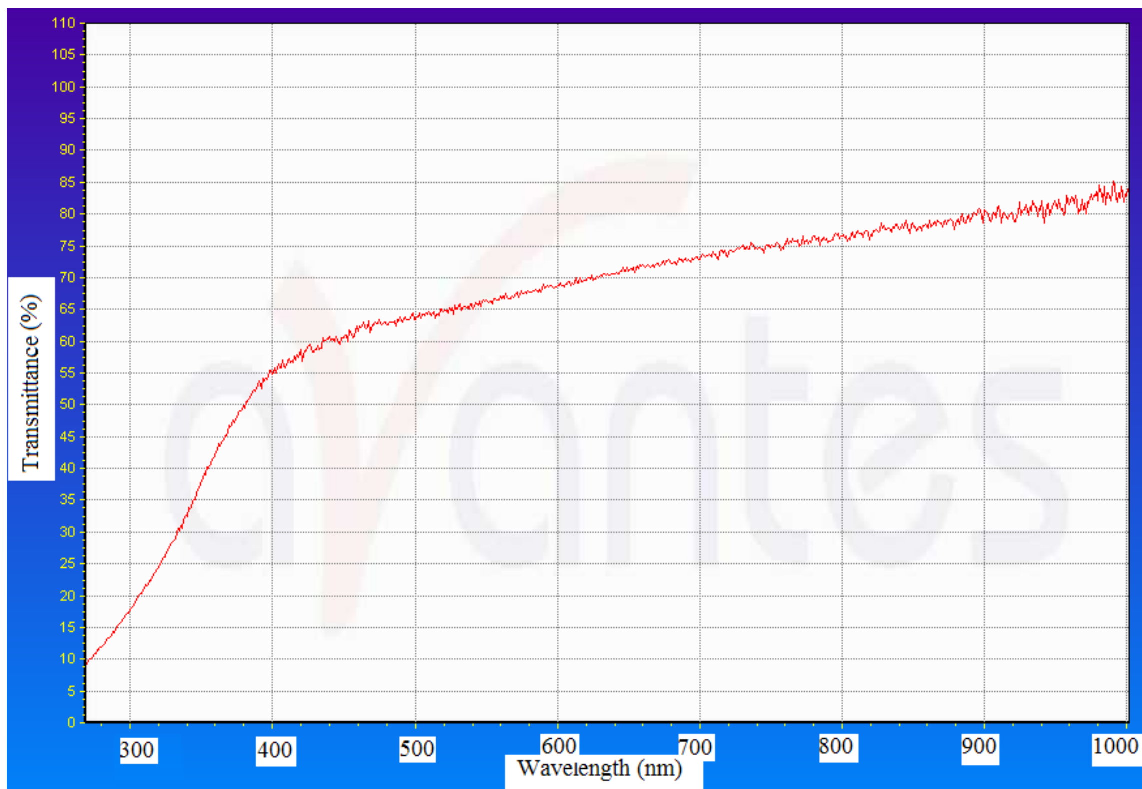

Figure 4.8: *Transmission spectra for sample 4 with 12% Cr. By extrapolate the abrupt change in the spectrum the band gap is estimated to 4.4 eV.*

Figure 4.9: *Transmission spectra for sample 5 with 7% Cr. By extrapolate the abrupt change in the spectrum the band gap is estimated to 2.8 eV.*

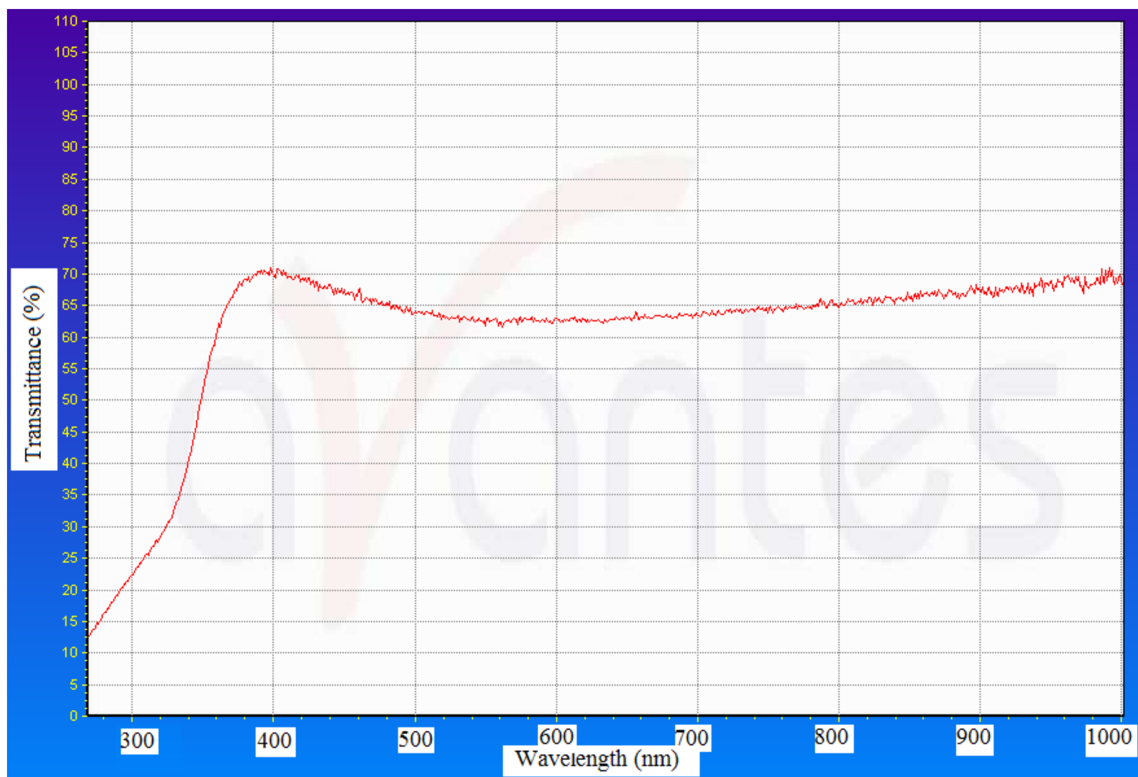

Figure 4.10: *Transmission spectra for sample 17 deposited on hot substrate with 4% Cr. By extrapolate the abrupt change in the spectrum the band gap is estimated to 4 eV.*

To analyze the samples without considering the thicknesses, the absorption coefficient is plotted against concentration for samples 1, 3, 4, 6, 8 and 10, containing 4%, 31%, 12%, 15%, 8% and 20% Cr respectively. A trendline is made to see how the concentration affects the absorption coefficent and is shown in Fig. (4.11). The trendline shows an increase of absorption for higher concentration of Cr. This is the same as found in [44]. The absorption coeffisient is found from Eq. (3.5) at 550 nm. The thickness of the samples are estimated from the profilometer, and the intensity is found from the transmission spectra in Fig. (4.4) and Fig. (4.3), taken with the old spectrophotmeter. However, the artifact seems only to interfer at low wavelengths, and the periodic dumps look to appear at same positions for all samples. We therefore believe that the absorption coefficient plot is reliable.

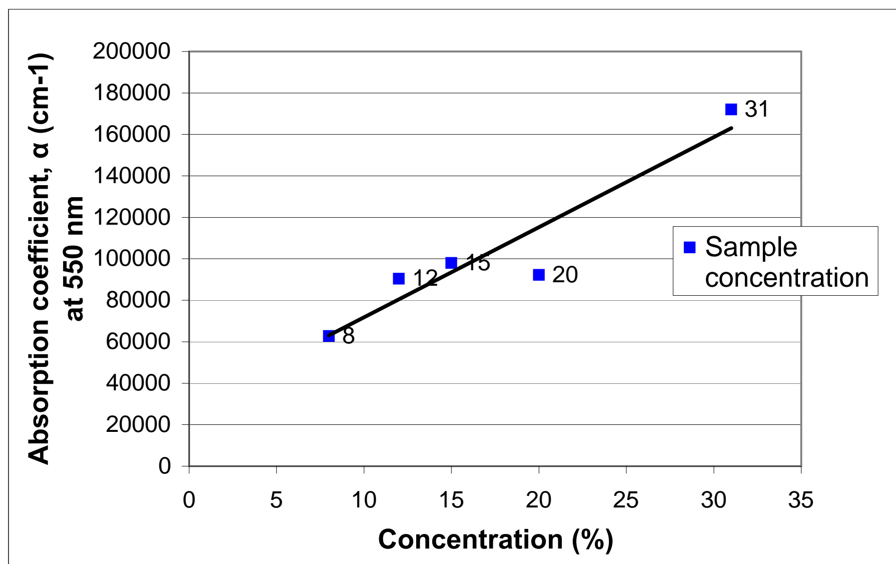

Figure 4.11: *The relationship between the absorption coefficient as a function of concentration. The trendline shows a linear increase in absorption coefficient with increasing doping concentration.*

As mentioned, the drop-off in transmission is at the band gap. The band gap can therefore be estimated from the spectra. Since the material absorbed all light beyond the band gap, the band gap occurs where the transmission intersects the x-axis. The band gap estimations are given in Table 4.2. The film on sample 2 did not transmit radiation down at the known band gap area for ZnS. The film looked metallic and opaque by eyes. The band gap could therefore not be calculated. The band gaps from sample 3, 4, 5 and 21

are estimated from the new spectrophotometer, while the rest is estimated based on the old one.

Table 4.2: *Estimated band gap from the visible spectrum of most of the samples. x denotes an unknown concentration, y denotes a drop in the transmission before the band gap was reached and z denotes that the band gap is below the observed range.*

No:	**% Cr**	**Band gap (eV)**
1	4%	3.78
2	21%	y
3	31%	z
4	12%	4.4
5	7%	2.8
6	15%	3.73
7	11%	3.72
8	8%	3.73
9	x	3.75
10	20%	3.76
11	x	3.73
12	x	3.83
13	x	3.76
14	x	3.72
15	x	3.82
17	x	4.0

For sample 3, 4, 9 and 11 the band gap is given in a Tauc plot. A Tauc plot is used to determine the band gap of materials. The plot is given as $(\alpha h\nu)^2$ vs. hν, where the α is estimated by Eq. (3.5), multiplied by hν and then squared. Since the plot is based on α, the samples are independent of their thicknesses. The plot is shown in Fig. (4.12).

Based on band gaps found in previous work for ZnS these band gaps tend to come from hexagonal structure. However, the band gaps variate little in the old spectrophotometer which indicate that the artifact plays a role at low wavelength. The intensity of the transmission is also lower at higher wavelength for the old spectrophotometer. There is however a change in the measured band gap which can be caused by an amorphous, a cubic or a mixed structure of the crystal for the different samples. A high concentration of Cr can also cause clusters of Cr instead of substitution with Zn, making the film insulating and raise the band gap. However, measurements in the

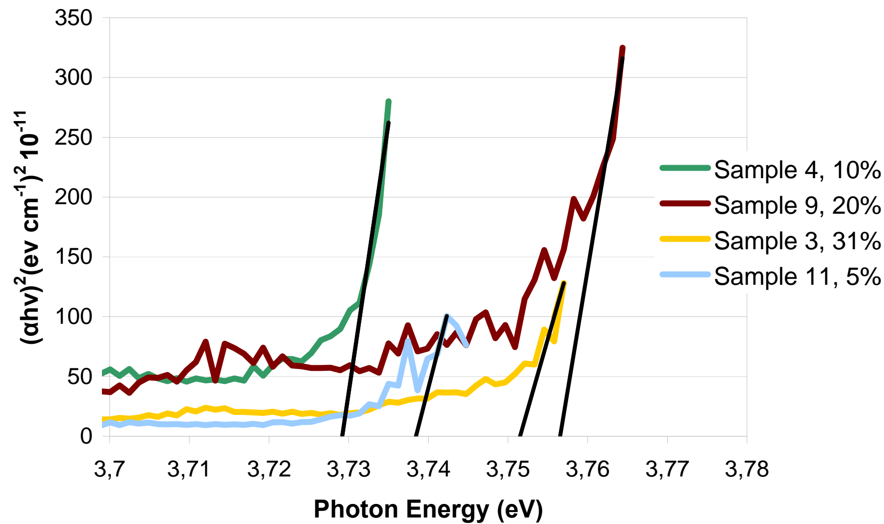

Figure 4.12: *The band gap is given where the trend line of the graphs intersects the x-axis. As can be seen there exists big deviations from each sample. However the band gap falls off in the range of pure ZnS.*

new spectrophotometer give another band gap estimation than from the band gap estimation from the old spectrophotometer. The new spectrophotometer gives more deviations from sample to sample based on the Cr concentration, especially for sample 3 where the band gap was not present. For the old spectrophotometer the band gaps seems to be more random distributed around the same value.

Sample 18, 19, 20 and 21, made on the backside of a Si wafer, are measured in the range from 1200-2500 nm in a spectrophotometer using diffuse reflectance. A clean back of a Si wafer is used as a reference. The measurements for sample 18, 19, 20 and 21 are given in Fig. (4.13(a)). Absorption occur for sample 18, 19 and 20 at 1400, 1700, 1950, 2150, 2300 and 2450 nm. From previous work a broad absorption peak from the Cr^{2+} shall only occur around 1700 nm [17]. Since the samples were to small to cover the pin hole they were fasten to a Si wafer with double sticky tape. Since the samples were unexpected to give absorption other places than at 1700 nm a measurement of a wafer with just a piece of tape was performed. The spectrum is shown in Fig. (4.13(b)). It can be seen that the absorption areas occurs for the same wavelengths for sample 18, 19 and 20 as for the Si wafer with tape. The difference in intensity is most likely caused since the measurements were

done with a different size of the tape piece. It is therefore tempting to believe that the absorption is due to the tape and not presence of Cr^{2+} in the sample. Sample 21 was on a big Si wafer which was big enough to fill the hole where the beam was reflected. The sample does not show any absorption lines, which agree well with other transmission spectra for pure ZnS [45].

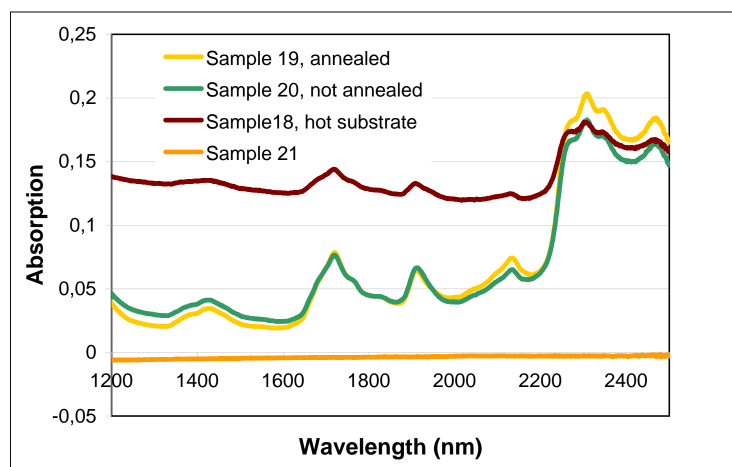

(a)

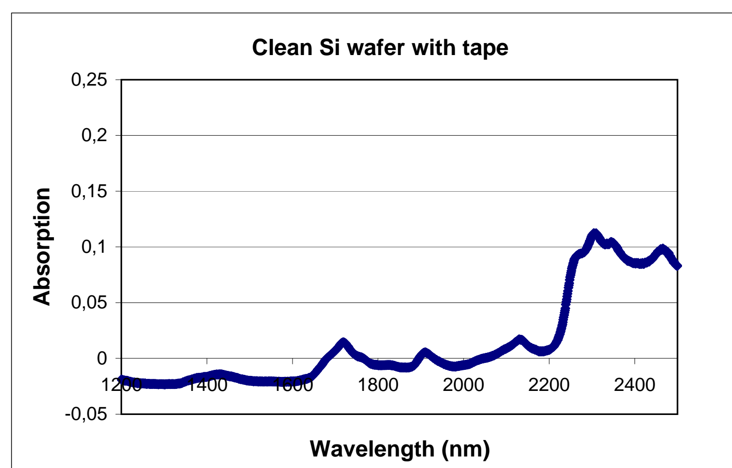

(b)

Figure 4.13: *Absorption of sample 18, 19 20 and 21. Sample 18-20 is attached to a clean Si wafer by double sticky tape. Sample 21 does not show any absorption band. In (b) an absorption spectrum of a Si wafer with a piece of double sticky tape. Compared to (a) the bands occur as a result of the double sticky tape.*

4.3 Wide range spectrum

Sample 3, 11 and 15 are investigated in the wide range from 250 nm to 3000 nm. The spectra are shown in Fig. (4.14). It can be seen that no absorption band occur. However, sample 3 has a more blunt absorption curve at low wavelengths compared to sample 11 and 15. As for Fig. (4.7(a)), a higher concentration of Cr seems to blunt the curve. Sample 15 and sample 11 shows an increasement in the absorption around 500 nm and 750 nm respectively. This corresponds to the ZnS transmission spectrum in Fig.(4.1), and interference fringes within the film. At 2600 nm water vapor absorption occur. The band gap seems to be a little lower in this measurements than in the measurements made in the old spectrophotometer for visible light, which support the assumption of a poor intensity in the light at low wavelengths or an artifact.

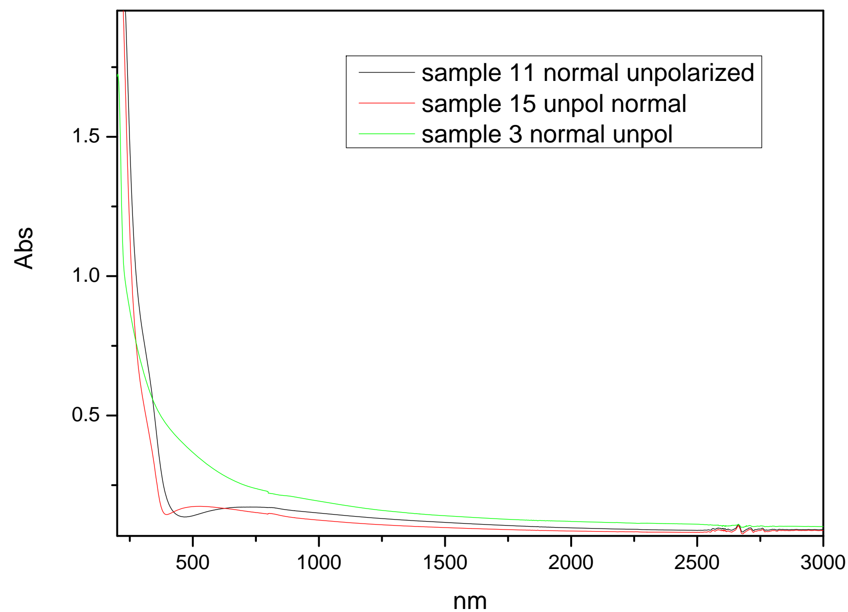

Figure 4.14: *Absorption spectra from 250 nm to 3000 nm. No band is found. However, the Cr affects the absorption giving a more blunt curve around 500 nm than the samples with lower Cr concentration. At 2600 nm absorption from water vapor is presence.*

4.4 FTIR

The samples are investigated in the region above 2500 nm. However, only a selection is shown in the spectra shown in Fig. (4.15). This concerns sample 2, 3, 4 and 5. The absorption at 2.74 μm for the pure ZnS sample is caused by the substrate, e.g. quartz. Sample 2, which is made on microscope glass, also drops around 2.5 μm before cut off at 5 μm due to the substrate. Sample 3, 4 and 5 are made on sapphire and drops off at 7.6 μm This is due to the absorption range of the substrate. Like expectations of absorption of ZnS:Cr from previous work from [17], no absorption bands occur.

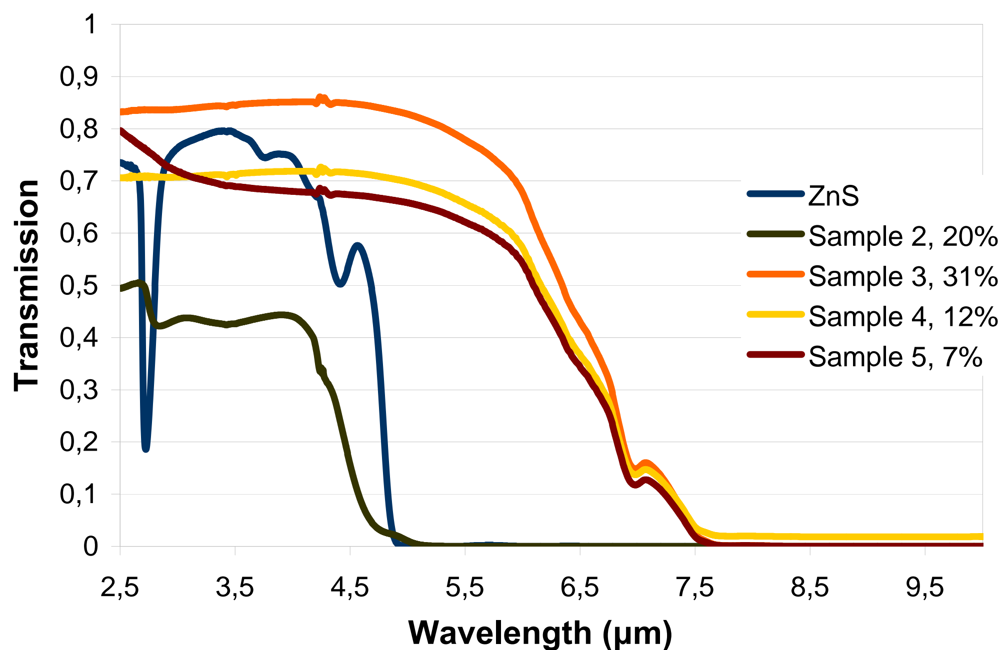

Figure 4.15: *Transmission spectrum as a function of wavelength from the FTIR. Only a selection of the samples is shown in the figure. The absorption lines are due to the substrates.*

4.5 XRD

Both the annealed and the non-annealed piece of sample 3 are investigated in XRD together with sample 4, sample 5, sample 17 and the annealed and non-annealed piece of sample 22. None of the samples showed any evident peaks for either a cubic or hexagonal structure of ZnS. A peak due to the substrate at 68.2 degree proved to be the [300] configuration of the substrate, and was only revealed for sample 3, 4 and 5. The reason why this peak only appeared at three samples can be due to bad cut of the sapphire substrate. The non-annealed sample 3 contain a little peak which can be seen at 29 degrees. Compared to the results in [30] this can be from the [111] peak in cubic or the [002] for the wurtzite structure. It is improbable that the peak comes from the substrate since sapphire does not have any configuration giving a peak at this angle. The most common possible configuration from sapphire is found in the data sheet shown in Appendix D.

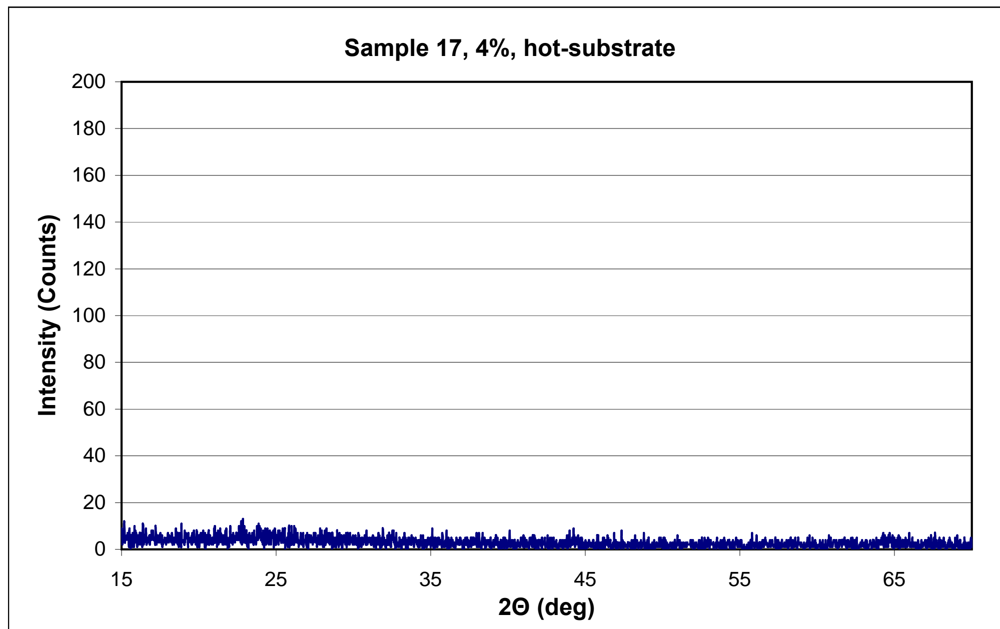

Figure 4.16: *XRD spectrum for sample 17 made on hot substrate. No peaks are observed. This may correspond to amorphous structure in the film.*

For the case of sample 17 and 22 no peaks are shown which implies an amorphous structure. Another reason for the absence of formation of lattice structure can be the thickness of the films. Mohamed et al. [29] reported amorphous structure of films below 50 nm. For thicknesses of 250 nm and 400 nm peaks of ZnS appeared. The film on sample 3, 4 and 17 can therefore be to thin to give evident peaks, but sample 5 and 22 should reveal peaks if the formation had lattice configuration.

The XRD spectrum reveled from Sample 17, where the film is deposited on a hot substrate, is shown in Fig. (4.16). The sample did not show peaks even for the substrate or the film. This highly implies that the sapphire is badly cut, e.g. not along the lattice, and an amorphous film. Subbaiah et.al [27] reported amorphous structure for films deposited on substrate above 350^0 C. As the temperature of the substrate can have been higher than what measured, e.g. 300^0 C, this can have caused amorphous structure also on the hot-temperature deposited film. The film may also have been to thin to reveal peaks.

Figure (4.17) shows the non-annealed sample in (a) and the annealed in (b). It is seen that the structure does not change during annealing. The substrate peak is shown at 68.2 degrees. In (a) a peak at 29 degrees can be observed. This can be a peak from the film for the [200] configuration of cubic ZnS or [101] from the wurtzite. This peak is absent after annealing, shown in (b). The same spectra as (b) reveals for sample 4 and 5 showing just the substrate peak.

Since none of the investigated ZnS:Cr samples showed a ZnS peak, sample 22 was investigated. Both the non-annealed and the annealed part. No substrate peak was expected since the film is deposited on fused silica. There is, however, not found a peak for either cubic or hexagonal structure in the films. This implies amorphous structure for the pure ZnS film. The spectrum is shown in Fig. (4.18).

Based on the results we were asking our self if we did anything wrong during these measurements. We highly doubt that because of spectra performed for another master's student. A spectrum of ZnO:Co on sapphire substrate is shown in Fig. (4.19). The spectrum shows peak for the [100] at 42 degrees configuration of sapphire and the [200] configuration for ZnO at 34 degrees. The [400] configuration can also be seen at 72 degrees.

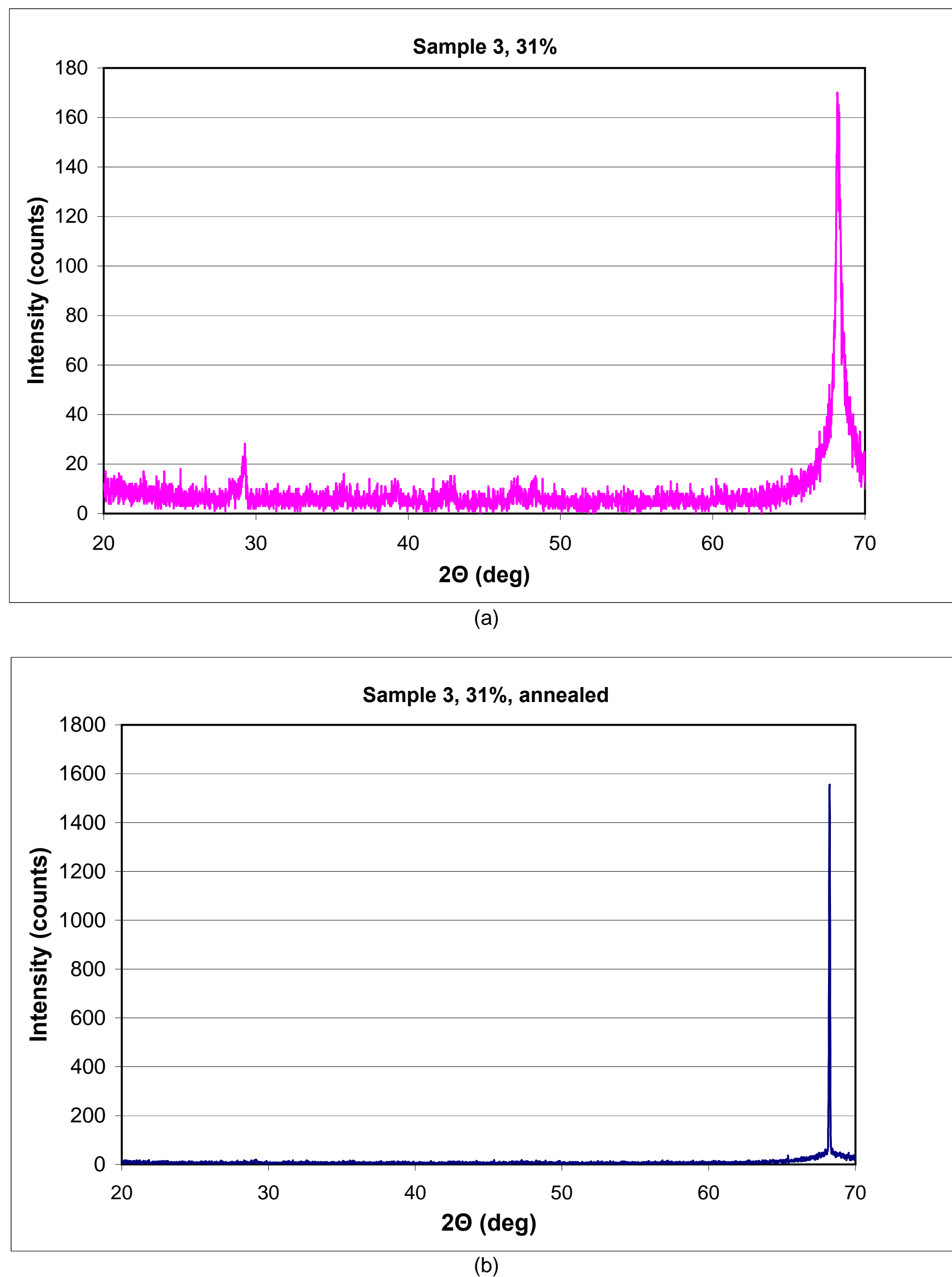

Figure 4.17: *XRD spectrum for sample 3. The non-annealed sample in (a) and the annealed in (b). The sapphire peak for the [300] configuration is shown at 68.2 degrees. The peak at 29 degrees in (a) can be the [111] configuration of ZnS. Note that number of counts are approximately 10 times higher in (b) than (a).*

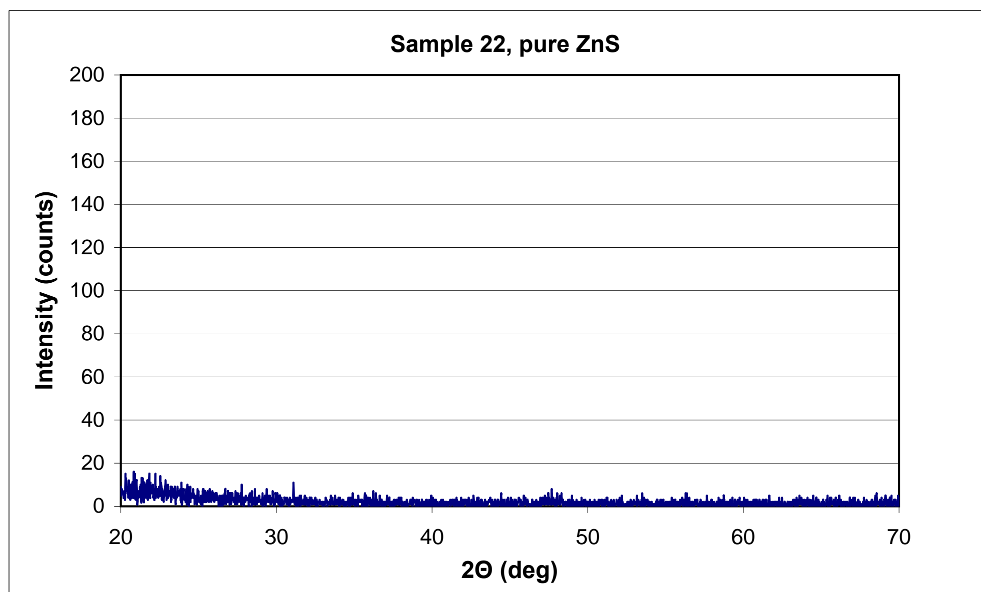

(a)

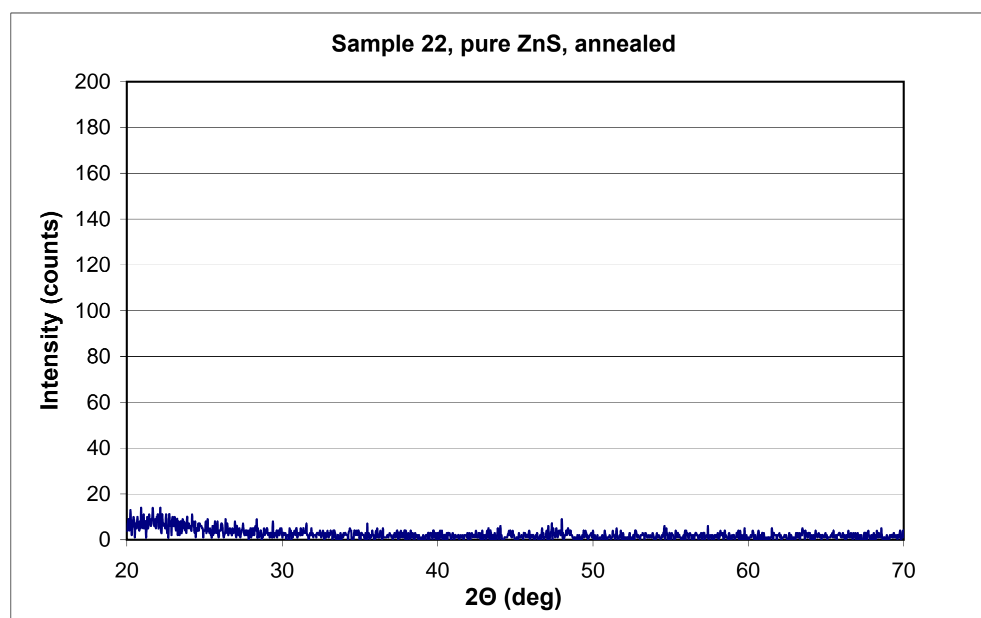

(b)

Figure 4.18: *XRD spectrum for sample 22. No peaks are observed, either before or after the annealing. There is however an increase in counts at low angles for both samples. This may correspond to amorphous structure in the film.*

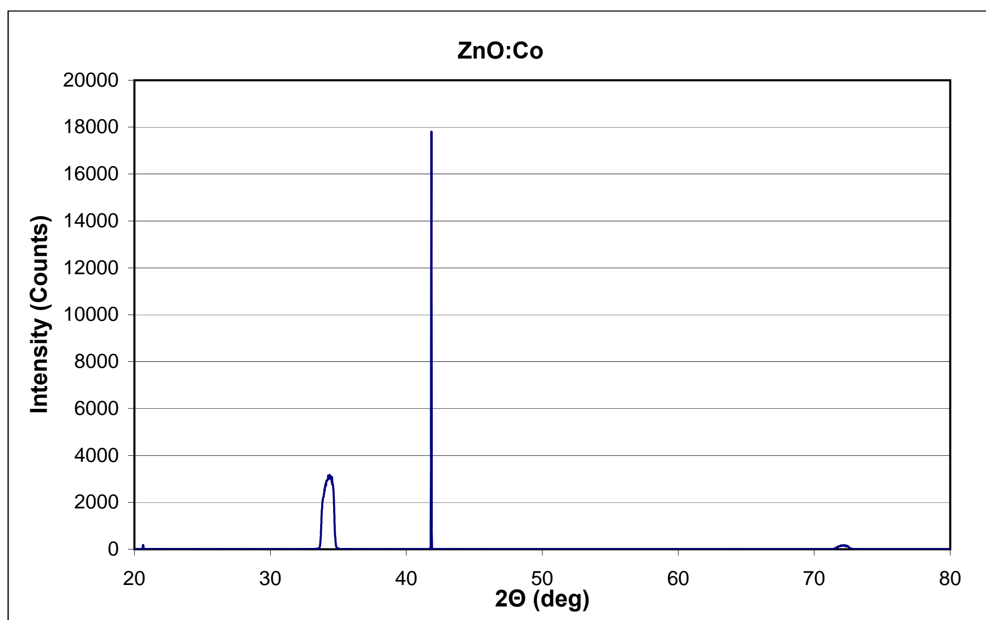

Figure 4.19: *Spectrum of ZnO:Co on sapphire substrate. The spectrum shows peaks for the [100] at 42 degrees configuration of sapphire and the [200] at 34 configuration for ZnO. The [400] configuration can also be seen at 72 degrees.*

4.6 AES

Sample 3, 5, 11 and 17 are investigated in Auger spectroscopy. O and C were present in all samples, together with Zn and S. The C and O are most likely somewhat due to post deposit contamination. Since O was present the signal from Cr can be obscured since the absorption of Cr and O appears at approximately the same energy. The samples was etched 2 nm with argon to remove the O and C. The effect from the substance decreased, but the sample still contained traces of Cr and O.

Sample 11, which should contain 5% of Cr, and sample 17 deposited on hot substrate did not show content of Cr. The latter should contain 80 Å Cr, however due to the hot substrate there might be an adhere problem which make it difficult for both Cr and ZnS to adhere. The samples also showed charging during the investigation which we interpret as an indication of poor conductivity. Figure (4.20(a)) shows a Scanning Electron Microscope (SEM) picture of sample 11. The picture for sample 17 loos the same. The horizontal lines are due to charging. The Auger spectrum for sample 11 is shown in Fig. (4.20(b)). It looks the same for sample 17.

Sample 3, containing 31% Cr, was also investigated. This sample showed a strong Cr absorption. Also sample 5 containing 7% Cr showed strong Cr absorption. From Fig. (4.21(a)) the SEM picture of sample 3 shows no charging problem, which indicates a conductive sample. The SEM picture of sample 5 looks the same. Figure (4.21(b)) shows the spectrum composition of sample 3. The Cr, Zn and S can easily be seen together with C and O. The same concerns sample 5.

Before depositions the base pressure were 8×10^{-6}. During deposition this rised to 1×10^{-5}. The O detected in the sample can come from O in the chamber during deposition. This will cause an interaction between Zn and make ZnO. C on the other hand contaminate the surface when materials are exposed for air. It is however usually easy to remove by etching with argon [46, p. 3].

(a)

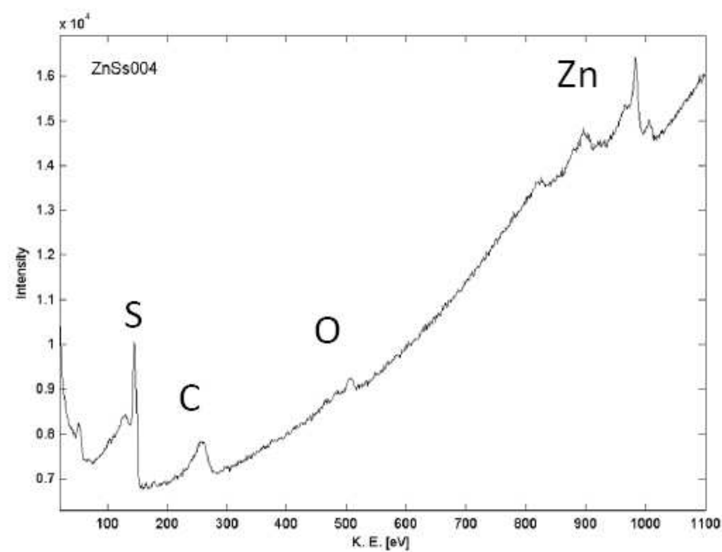

(b)

Figure 4.20: *A SEM picture in (a) and the thin film composition in (b) for sample 11. Picture (a) reveals a charging problem in the sample, e.g. non-conducting film. From picture (b) it can be seen that Cr does not appear in the sample.*

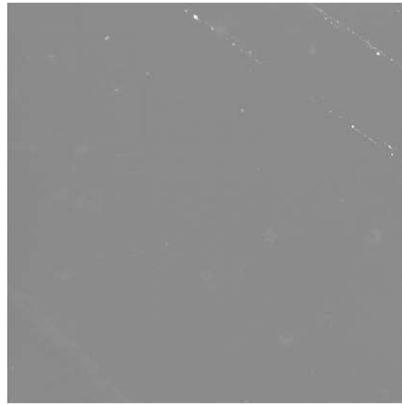

(a)

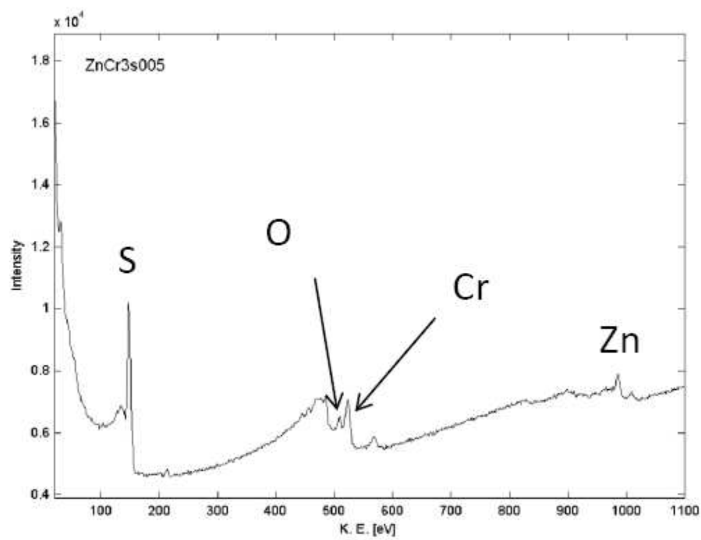

(b)

Figure 4.21: *A SEM picture in (a) and the thin film composition in (b) of sample 3. No charging problem occur as can be seen from picture (a). The sample contain Cr as can be seen from picture (b).*

4.7 Hall-measurement and four probe measurement

Hall measurement was performed on sample 3 and 4. None of the samples showed a free carrier density. Four-probe measurement was performed on sample 1 - 15. The result confirmed the assumption of non-conductive samples from the Hall-measurement. The poor conductivity has been reported earlier from [19], especially when the level of impurities exceed 0.1 mole %. During Auger measurement sample 11 showed a build up charge which also implicate non-conductivity. Sample 3 did not show this build up energy and showed conductivity. However, the sample did not show conductivity even with a 20MΩ two point probe.

Chapter 5

Conclusion and future work

In this thesis a setup of vacuum system for co-deposition was used for production of ZnS:Cr films. The films were of varying thicknesses and doping levels. The incorporation of Cr was in optically inactive sites and seemed to make the films more insulating. Both annealing and and deposition onto hot substrates were unsuccessful in producing absorption from Cr^{2+}.

The films were investigated with a profilometer and the doping concentrating was determined from these measurements. Sample of lower concentration than 7% could not be estimated. It is found that the thicknesses of the films strongly depends on where they are located in the deposition chamber. To measure the transmission of the films they are investigated in five spectrophotometers with overlapping ranges, three in visible, two in NIR and one FTIR. All measurements imply non-conducting samples and hopping conductivity. Most likely because of incorporation of Cr clusters. This is concluded from that the band edge is meared out at shorter wavelength than pure ZnS in the visible range and that the films showed no conductivity in four probe measurement. For a 3340 Å thick 7% sample the band structure seemed to disrupt making the band gap at higher wavelengths. The sample still showed no conductivity in four-probe measurement and amorphous structure was revealed in XRD.

No Cr^{2+} absorption was found from samples made on Si in the NIR infrared spectra either. Neither for the annealed sample, sample deposited on hot substrate or the sample deposited in room temperature. No IR reflectivity was found in neither high concentrated samples or low concentrated samples.

Both measurements support the assumption of incorporation of Cr clusters.

XRD did not reveal peaks in scans from 20-70 degrees except for one sample with low counts for the [111] peak for cubic or [002] for the wurtzite lattice configuration. Amorphous structure in the films are concluded in the other films, but small-scattering effects in ZnS and small amts off Cr can play a role in formation of the structure. However, no structure was found for a sample with pure ZnS, both before and after annealing.

Auger confirmed the presence of Cr in some samples, but the surface concentration was lower than expected. This may be due migration of Cr into the film making Cr clusters. For the hot substrate deposition there might be an adhere problem. The films showed traces after O and C. As Cr and O will give of Auger electrons at about the same energy low amount of Cr can be hard to find. Charging in the Auger was a problem, but high concentrated sample of 31% showed reduced charging. The sample showed however no conductive properties from Hall-meausurement, four-probe measurement or from a two-point configuration with 20 MΩ resistance. The sample showed also a broadband absorption with no evidence of the ZnS band gap. None of the other samples showed neither conductive properties from four-probe measurement. This support the suspicion of Cr clusters at inactive sites, which seem to make the films more insulating.

To continue the research of ZnS:Cr films made by PVD there are several ways to go. Even though no samples showed formation and incorporation of Cr^{2+} in this project, there are several teqnuiches which will give important information of the ZnS:Cr films and proposal to how to make them better. Diffuse reflectance on the backside of Si wafers showed a great potential for the investigation on films that may not have perfect optical quality. As the room temperature deposition more or less failed, and the annealing gave cracks in the film, new films on hot substrate of various concentration can be made on the Si wafer and investigated with diffuse reflectance. A suggestion is to lower the temperature, or calibrate the heater to 300° C, to see if ZnS and Cr may adhere better to the substrate and also incorporate Cr^{2+} into ZnS. As the 3340 Å 7% film showed disruption of the band gap at higher wavelenght, and that intermediate band in p-i-n materials should be in range around 200 nm, more films around 1500-3000 Å should be tried out with Cr concentration from 1%-15%. Measurements of cathodeluminescence or photoluminescence to characterize for estimation of the band gap can also be performed. Also Optical Detection of Magnetic Resonance (ODMR), Electron Paramagnetic Resonance (EPR) or Electron Spin Resonance (ESR) spectroscopy can be

performed to give information of the role Cr plays in radiative processes in ZnS:Cr deposited by PVD.

Surface analysis of the samples can also give valuable information of the sample structures. This can be done by AFM and Scanning Transmission Electron Microscope (S(T)EM). The determination of Cr in the films are made through estimation from profilometer and the rate monitors. To evaluate the accuracy of the deposition rate and the concentration of Cr in the sample EDX or X-ray photoelectron spectroscopy (XPS) could be performed on the samples. Especially since the AES did not show any trace of Cr in some samples. This will however be difficult to perform on samples made on rough Si wafers.

If Cr^{2+} is managed to incorporate in ZnS the succeed of making ohmic contacts would be a step in the right direction making a solar cell. As ohmic contacts in ZnS has shown difficulties this must be overcome. If we manage to obtain ohmic contacts, making a solar cell module and characterizise current-voltage (I-V) curves can give an indication of the existence of an IB in the ZnS:Cr. And further the possibility that one day in the future common solar cells are made from ZnS with an IB made from Cr.

Bibliography

[1] J. Twidell and T. Weir, *Renewable Energy Resources.* Taylor & Francis Ltd, second ed., 2006.

[2] A. Shah, P. Torres, R. Tscharner, N. Wyrsch, and H. Keppner, "Photovoltaic technology: the case for thin-film solar cells," *Science*, vol. 285, no. 5428, p. 692, 1999.

[3] A. Goetzberger, J. Luther, and G. Willeke, "Solar cells: past, present, future," *Solar energy materials and solar cells*, vol. 74, no. 1-4, pp. 1–11, 2002.

[4] R. Strandberg, *Theoretical studies of the intermediate band solar cell.* PhD thesis, 2010.

[5] M. Green, *Third Generation Photovoltaics : Advanced Solar Energy Conversion.* Springer-Verlag Berlin Heidelberg, 2006.

[6] A. Luque and A. Martí, "Increasing the efficiency of ideal solar cells by photon induced transitions at intermediate levels," *Physical Review Letters*, vol. 78, no. 26, pp. 5014–5017, 1997.

[7] A. Luque, A. Martí, A. Bett, V. Andreev, C. Jaussaud, J. Van Roosmalen, J. Alonso, A. Rauber, G. Strobl, and W. Stolz, "FULLSPECTRUM: a new PV wave making more efficient use of the solar spectrum," *Solar energy materials and solar cells*, vol. 87, no. 1-4, pp. 467–479, 2005.

[8] K. Seeger, *Semiconductor Physics.* Springer-Verlag Berlin Heidelberg New York, 9 ed., 2004.

[9] L. Wang and A. Zunger, "Cluster-doping approach for wide-gap semiconductors: The case of p-type ZnO," *Physical review letters*, vol. 90, no. 25, p. 256401, 2003.

[10] B. G. Streetman and S. K. Banerjee, *Solid State Electronic devices.* Pearson International Edition, sixth ed., 2010.

[11] S. Elliott, *The physics and chemistry of solids.* John Wiley & Sons, 2008.

[12] A. Luque and A. Martí, “The intermediate band solar cell: Progress toward the realization of an attractive concept,” *Advanced Materials*, vol. 22, no. 2, pp. 160–174, 2010.

[13] L. Cuadra, A. Marti, and A. Luque, “Present status of intermediate band solar cell research,” *Thin solid films*, vol. 451, pp. 593–599, 2004.

[14] D. Kruangam, M. Deguchi, T. Toyama, H. Okamoto, and Y. Hamakawa, “Carrier injection mechanism in an a-SiC p-i-n junction thin-film LED,” *Electron Devices, IEEE Transactions on*, vol. 35, no. 7, pp. 957–965, 1988.

[15] T. Bergstresser and M. Cohen, “Electronic structure and optical properties of hexagonal CdSe, CdS, and ZnS,” *Physical Review*, vol. 164, no. 3, p. 1069, 1967.

[16] Y. Li, Z. Zhou, P. Jin, Y. Chen, S. Zhang, and Z. Chen, “Achieving Ferromagnetism in Single-Crystalline ZnS Wurtzite Nanowires via Chromium Doping,” *The Journal of Physical Chemistry*, no. 114, pp. 12099–12103, 2010.

[17] I. T. Sorokina, “Cr^{2+}-doped II-VI materials for lasers and nonlinear optics,” *Optical Materials*, no. 26, pp. 395–412, 2004.

[18] J. Zhang, J. Ding, J. Cao, and Y. Zhang, “Infrared, visible and ultraviolet absorptions of transition metal doped ZnS crystals with spin-polarized bands,” *Journal of Solid State Chemistry*, 2010.

[19] S. Sharma and R. Singh, “Electrical conductivity of doped ZnS,” *Bulletin of Materials Science*, vol. 14, no. 1, pp. 71–75, 1991.

[20] H. Nelkowski and G. Grebe, “IR-luminescence of ZnS:Cr,” *Journal of Luminescence*, vol. 1, pp. 88–93, 1970.

[21] C. Tablero, “Correlation and nuclear distortion effects of Cr-substituted ZnSe,” *The Journal of chemical physics*, vol. 126, p. 164703, 2007.

[22] T. Enomoto and W. Anderson, "Investigation on trap distribution and photoelectronic effect due to UV, IR and visible light excitation in self-activated ZnS crystals," *Journal of Physics and Chemistry of Solids*, vol. 38, no. 3, pp. 247–253, 1977.

[23] N. Vlasenko, P. Oleksenko, Z. Denisova, M. Mukhlyo, and L. Veligura, "Cr-related energy levels and mechanism of Cr^{2+} ion photorecharge in ZnS:Cr," *Physica Status Solidi (b)*, vol. 245, no. 11, pp. 2550–2557, 2008.

[24] C. Tablero, "Electronic and magnetic properties of ZnS doped with Cr," *Physical Review B*, vol. 74, no. 19, p. 195203, 2006.

[25] Y. Brada, "Electrical conductivity of ZnS crystals: ZnS crystals as quasi-one-dimensional conductors," *Physical Review B*, vol. 39, no. 11, p. 7645, 1989.

[26] M. Nadeem and W. Ahmed, "Optical Properties of ZnS thin films," *Turkish Journal of Physics*, vol. 24, pp. 651–659, 2000.

[27] Y. Subbaiah, P. Prathap, and K. Reddy, "Structural, electrical and optical properties of ZnS films deposited by close-spaced evaporation," *Applied Surface Science*, vol. 253, no. 5, pp. 2409–2415, 2006.

[28] J. Cheng, D. Fan, H. Wang, B. Liu, Y. Zhang, and H. Yan, "Chemical bath deposition of crystalline ZnS thin films," *Semiconductor science and technology*, vol. 18, p. 676, 2003.

[29] S. Mohamed, M. El-Hagary, and M. Emam-Ismail, "Thickness and annealing effects on the optoelectronic properties of ZnS films," *Journal of Physics D: Applied Physics*, vol. 43, p. 075401, 2010.

[30] A. Kassim, S. Nagalingam, H. Min, and N. Karrim, "XRD and AFM studies of ZnS thin films produced by electrodeposition method," *Arabian Journal of Chemistry*, vol. 3, no. 4, pp. 243–249, 2010.

[31] Mattox, D.M. and ScienceDirect (Online service), *Handbook of physical vapor deposition (PVD) processing.* William Andrew, 2010.

[32] J. M. Bennett and L. Mattsson, *Introduction to Surface Roughness and Scattering.* Optical Society of America, 2 ed., 1999.

[33] `http://www.fc.up.pt/pessoas/peter.eaton/tutorial/toc.html`, 14.05.2011.

[34] E. N. Kaufmann, *Characterization of Materials*, vol. 2. John Wiley & Sons, 1 ed., 2003.

[35] W. Zhou and Z. L. Wang, *Scanning Microscopy for Nanotechnology, Techniques and Applications*. Springer, 2007.

[36] M. Quirk and J. Serda, *Semiconductor Manufacturing Technology, Chapter 7*. Prentice-Hall, 2001.

[37] A. Ashour, H. Afifi, and S. Mahmoud, "Effect of some spray pyrolysis parameters on electrical and optical properties of ZnS films," *Thin solid films*, vol. 248, no. 2, pp. 253–256, 1994.

[38] M. Rothschild, D. Ehrlich, and D. Shaver, "Effects of excimer laser irradiation on the transmission, index of refraction, and density of ultraviolet grade fused silica," *Applied physics letters*, vol. 55, no. 13, pp. 1276–1278, 1989.

[39] V. Chandrasekharan and H. Damany, "Birefringence of sapphire, magnesium fluoride, and quartz in the vacuum ultraviolet, and retardation plates," *Applied Optics*, vol. 7, no. 5, pp. 939–941, 1968.

[40] W. Schrenk and J. Wheatley, "Infrared reflective optical interference film.," Feb. 5 1992. EP Patent 0,469,732.

[41] `http://en.wikipedia.org/wiki/File:Helium$_$spectrum.jpg`, 08.06.2011.

[42] M. Van Staveren, H. Brom, and L. De Jongh, "Metal-cluster compounds and universal features of the hopping conductivity of solids," *Physics reports*, vol. 208, no. 1, pp. 1–96, 1991.

[43] P. Krulevitch, A. Lee, P. Ramsey, J. Trevino, J. Hamilton, and M. Northrup, "Thin film shape memory alloy microactuators," *Microelectromechanical Systems, Journal of*, vol. 5, no. 4, pp. 270–282, 1996.

[44] J. Vallin, G. Slack, S. Roberts, and A. Hughes, "Infrared absorption in some II-VI compounds doped with Cr," *Physical Review B*, vol. 2, no. 11, p. 4313, 1970.

[45] `http://www.internationalcrystal.net/optics_19.htm`, 08.06.2011.

[46] M. W. J, *Methods of surface analysis*. Cambridge University Press, 1989.

List of Figures

2.1 *Typical band structures for insulators, semiconductors and metals at 0 K. The insulator has a wide band gap so electrons can not get excited across. A semiconductor has a more narrow band gap so photons get excite the electrons across the band gap, while metals does not contain a band gap so they conduct easily* [10, Based on figure 3-4]. 4

2.2 *The establishment of the Fermi-level in an intrinsic material. From the Fermi-Dirac distribution the probability of finding an occupied state with the Fermi energy is equal 1/2, making the Fermi-level in the middle of the band gap.* 5

2.3 *The band alignment of a semiconductor at 0K in (a). In (b) electrons have been exited by absorption of photons, optical or thermal. The process is called an electron-hole generation.* . . 6

2.4 *The* ***k*** *space for an direct band gap in (a) and an indirect band gap in (b). The electron falling from the CB to the VB in (b) undergoes a change in the momentum.* [10, Based on figure 3-5]. 7

2.5 *A partially filled donor level is created near the CB at 0K by donor-doping. When the temperature increases the electrons can get excited easily across the band gap.* [10, Based on figure 3-12 (a)]. 8

2.6 *A creation of an empty acceptor band created by doping in (a). (b) shows how electrons easily can excite up in the band, this can occur even at low temperature.* [10, Based on figure 3-12 (b)]. 8

2.7 *The Fermi-level is dependent on the doping level in the material. (a) shows the Fermi level in a p-doped material, while (b) shows for n-doped material.* [10, Based on Figure 3-15]. . . 9

2.8 *Schematic of the depletion region and how an E-field are established when a p and n material is junctioned together.*[10, Based on figure 5-11]. 10

2.9 *Creation of a pn-junction and the affection on the Fermi-level and the band alignment. (a) shows two opposite doped semiconductors before the junction is established. (b) shows the band bending to keep the Fermi level constant throughout the system, while (c) shows how a depletion region and quasi-Fermi levels are established.* [4, Based on Figure 2.6]. 11

2.10 *An ideal heterojunction between a wide band gap p-type material and a more narrow n-type material. Figure (a) shows the bands before they are aligned. As can be seen the Fermi level of the p-type material is below the VB for the n-type material. This is also shown for the band alignment in (b). Discontinuities in the conduction and VB are created for the Fermi-level to be constant.* [10, Based on figure 5-45]. 13

2.11 *Excited electrons can be utilized in an external circuit to create current flow. An incoming photon excites electron from the VB to the CB. Excited electrons is driven to an external circuit and back to the VB. The gap between the electrochemical potential in the VB and CB is the limit of extracted current.* [4, Based on Figure 2.2]. 14

2.12 *How photons interacts with electrons and excite them in the CB. Photons with less energy than band gap energy (1) continue through the material, photons with energy equal band gap energy excite electrons without losses (2), while photons with energy above band gap energy undergo heat exchange in the relaxation within the CB (3)* [4, Based on figure 2.5]. 15

2.13 *Black body radiation from a 5250 ^{0} C surface, black line, the sunlight at the top of the atmosphere, the yellow area and the incoming radiation at the sea level, the red area. The figure also shows the absorption band for H_2O, O_2 and CO_2.* 17

2.14 *Shows the to step transition of the excitation. The excitation from the VB to the IB, labeled E_{g1}, from the IB to the CB, labeled E_{g2}, and from the VB to the CB, labeled E_g3.* [4, Based on Figure 3.1]. 18

2.15 *Shows the quasi-Fermi levels for the CB, VB and IB. It also shows the three excitation possibilities and the direction of the utilized voltage.* Based on figure [12, 1(b)] and [13, 1(b)]. . . . 19

2.16 *The two main structure of ZnS, sinc blende (left) and wurtzite (right).* 22

2.17 *An absorption spectrum of ZnS:Cr, ZnSe:Cr and CdSe:Cr. The absorption of Cr_{2+} in ZnS appear at 1700 nm. The figure is taken from* [17]. 23

2.18 *Lattice defects for Cr substituted with Zn. The different Cr^{2+} and Cr^{+} ions shows traps and levels at different energy levels within the band gap. The energy levels can work as transition places for an IB between the valence and CB. The figure is taken from* [23]. 24

2.19 *Diffracted peaks for ZnS films made with E-beam evaporator. The left figure shows the diffraction pattern for different sample thicknesses. The right shows how annealing effects the sample of 400 nm. Figure taken from* [29]. 26

2.20 *XRD plot of ZnS deposited by electrodeposition for 15 minutes. The white markers show the diffraction from the substrate, $In_{1.875}O_3Sn_{0.125}$. The black markers show the diffraction from the ZnS. The revealed configurations imply cubic structure. Graph (a) is from the film grown at -1V potential, graph (b) was grown at -1.1V and graph (c) for the film grown at -1.3V. Figure taken from* [30]. 27

3.1 *The principles behind an XRD system. The source is fixed, while the sample holder and detector are moving. As the sample moves an angle θ, the detector moves 2θ. When X-rays collide with electrons in the lattice a diffraction pattern can be revealed.* 37

3.2 *Schematic description of how the Hall-measurement. A sample is placed in a magnetic field in the B_z direction and a current is sent in the I_x direction. This induce an electric field, the Hall-effect, between A and B, marked E_y.* 39

3.3 *Schematic description of a Four probe measurement. A probe with four contacts is pushed down on the sample. A current is applied between two of the probes when the to others measuring the voltage between the two others.* 40

3.4 *Schematic description of the deposition chamber. To source are divided by a partition wall. The substrate is placed above the sources. Next to the substrate two quartz crystal monitors measure the rate for each of the sources.* 42

4.1 *Shows the transmission spectrum for a model made from 900Å thick ZnS on quarts. In (b) the measured spectrum is showed as a function of wavelength through a 1000 Å thick ZnS film made on $Si0_2$ substrate. The increase in transmission at lower wavelength is due due to interference in the film.* 50

4.2 *Transmission spectra for sample 5, 9, 11, 14 and 15 deposited on sapphire as a function of wavelengths.* 51

4.3 *Transmission spectra for sample 3, 4 and 7 deposited on sapphire as a function of wavelengths.* 52

4.4 *Transmission spectra for sample 6, 8, 10, 12, 13 deposited on fused silica as a function of wavelengths.* 53

4.5 *(a), the He-spectrum from the spectrophotometer. (b), a specter of where He-lines shall occur. Figure (b) taken from* [41] . . . 54

4.6 *The ZnS film on fused silica before annealing in (a). No big cracks are observed. In (b) the same sample is shown after annealing. Several big cracks can be observed.* 56

4.7 *The transmission spectra for sample 3. (a) shows the non-annealed sample of 31% Cr and (b) the same sample after annealing. There is no big deviations from the figures, and both seems insulating with a high band gap.* 57

4.8 *Transmission spectra for sample 4 with 12% Cr. By extrapolate the abrupt change in the spectrum the band gap is estimated to 4.4 eV.* 58

4.9 *Transmission spectra for sample 5 with 7% Cr. By extrapolate the abrupt change in the spectrum the band gap is estimated to 2.8 eV.* 59

4.10 *Transmission spectra for sample 17 deposited on hot substrate with 4% Cr. By extrapolate the abrupt change in the spectrum the band gap is estimated to 4 eV.* 60

4.11 *The relationship between the absorption coefficient as a function of concentration. The trendline shows a linear increase in absorption coefficient with increasing doping concentration.* 61

4.12 *The band gap is given where the trend line of the graphs intersects the x-axis. As can be seen there exists big deviations from each sample. However the band gap falls off in the range of pure ZnS.* 63

4.13 *Absorption of sample 18, 19 20 and 21. Sample 18-20 is attached to a clean Si wafer by double sticky tape. Sample 21 does not show any absorption band. In (b) an absorption spectrum of a Si wafer with a piece of double sticky tape. Compared to (a) the bands occur as a result of the double sticky tape.* . . . 64

4.14 *Absorption spectra from 250 nm to 3000 nm. No band is found. However, the Cr affects the absorption giving a more blunt curve around 500 nm than the samples with lower Cr concentration. At 2600 nm absorption from water vapor is presence.* . . 65

4.15 *Transmission spectrum as a function of wavelength from the FTIR. Only a selection of the samples is shown in the figure. The absorption lines are due to the substrates.* 66

4.16 *XRD spectrum for sample 17 made on hot substrate. No peaks are observed. This may correspond to amorphous structure in the film.* 67

4.17 *XRD spectrum for sample 3. The non-annealed sample in (a) and the annealed in (b). The sapphire peak for the [300] configuration is shown at 68.2 degrees. The peak at 29 degrees in (a) can be the [111] configuration of ZnS. Note that number of counts are approximately 10 times higher in (b) than (a).* 69

4.18 *XRD spectrum for sample 22. No peaks are observed, either before or after the annealing. There is however an increase in counts at low angles for both samples. This may correspond to amorphous structure in the film.* 70

4.19 *Spectrum of ZnO:Co on sapphire substrate. The spectrum shows peaks for the [100] at 42 degrees configuration of sapphire and the [200] at 34 configuration for ZnO. The [400] configuration can also be seen at 72 degrees.* 71

4.20 *A SEM picture in (a) and the thin film composition in (b) for sample 11. Picture (a) reveals a charging problem in the sample, e.g. non-conducting film. From picture (b) it can be seen that Cr does not appear in the sample.* 73

4.21 *A SEM picture in (a) and the thin film composition in (b) of sample 3. No charging problem occur as can be seen from picture (a). The sample contain Cr as can be seen from picture (b).* 74

B.1 *Shows the to step transition of the excitation. The excitation from the valence band to the intermediate band, labeled E_{g1}, from the intermediate band to the conduction band, labeled E_{g2}, and from the valence band to the conduction band, labeled E_g3.* [4, Based on Figure 3.1]. 100

C.1 *An overview over the deposition system, better known as "The Beast".* 102

C.2 *An overview inside the deposition chamber. As seen the sources are ...* 102

List of Tables

4.1 *The data from the monitors during deposition and the profilometer after the deposition. As can be seen there is a deviation for the wanted deposition concentration and the post-examination. For the samples were the concentration could not be estimated from the profilometer an x is denoting the concentration.* 47

4.2 *Estimated band gap from the visible spectrum of most of the samples. x denotes an unknown concentration, y denotes a drop in the transmission before the band gap was reached and z denotes that the band gap is below the observed range.* 62

Appendix A

Detailed balance of solar cell physics

When calculating the maximum possible efficiency of a solar cell it is the number of photons being emitted from and absorb in the cell that is calculated. The difference represents the number of electrons which can be driven through the external circuit [4].

For an single gap solar cell Eq (A.1) can be used to calculate the radiative recombination for a cell with infinite thickness. The emission of photons per unit time per unit area will be given as

$$R = \frac{2\pi}{h^3c^2}\int_{E_L}^{E_H} \frac{\alpha(E_\gamma)E_\gamma^2}{e^{(E_\gamma-\Delta\mu)/kTc}-1}dE_\gamma \tag{A.1}$$

where h is Planck's constant, c the speed of light, $\alpha(E_\gamma$ is the absorption coefficient for photons with energy E_γ, $\Delta\mu$ is denotes the splitting between the quasi-Fermi, e.g. the level for electrons and holes in the conduction band and valence band respectively, k Boltzmann's constant and T_c the temperature of the solar cell, typically 300K. The limits for the integration denotes $E_L = E_g$ and $E_H = \infty$.

The incoming radiation towards the cell can come from either an optical system used to concentrate the sun or the the sun itself. Since the ambient is not at 0 K the thermal radiation from the surroundings will also contribute

in electron-hole pairs generation. The number of photons containing energy E_γ that are emitted by a black body with temperature T_r per unit time, surface, solid angle and energy are given as

$$N(E_\gamma, T_r) = \frac{2}{h^3c^2}(\frac{E_\gamma^2}{e^{E_\gamma/kT_r - 1}}) \tag{A.2}$$

Using the black body simplification the number of photons emitted by the sun can be calculated.

$$\Phi(E_\gamma) = \phi[Xsin^2\Theta_{sun}N(E_\gamma, T_s + (1 - Xsin^2\Theta_{sun})N(E_\gamma, T_a)] \tag{A.3}$$

where X denotes the number of suns, X_{max}=1/sin$^2\theta_{sun}$=46050, which is the incoming solar radiation over the entire hemisphere above the front surface, θ_{sun} is the suns semiangle seen from the sun $\approx 0.267^0$, T_s is the sun temperature and T_a is the ambient temperature.

Now it is time to sum up the maximum effiency from a solar cell. Assuming that no photon beyond the band gap energy generates electron-hole pairs and that all of the photons above do the generation per unit area for an infinitely thick cell becomes

$$G = \int_{E_g}^{\infty} a(E_\gamma \Phi(E_\gamma) dE_\gamma \tag{A.4}$$

where $a(E_\gamma$ can be set to either 1 or 0 for an infinitely thick cell.

As both the generation and recombination of the electron-hole pairs are established, the theoretical current density, J, of a solar cell can be calculated. The number pf electrons excited must be equal to the sum of the electrons that are harvested and the electrons which are deexcited. This gives the current density of a solar cell as

$$J = q(G - R) \tag{A.5}$$

where q denotes as the elementary charge.

For a optimal splitting of the quasi-Fermi levels the cell voltage V_m is the voltage with a highest possible efficiency the cell can deliver. This efficiency is given as

$$\eta = \frac{J_m V_m}{E_{in}} = \frac{J_m V_m}{\pi X sin^2\theta_{sun} \int_0^\infty E_\gamma N(E_\gamma, T_s) dE_\gamma} \tag{A.6}$$

where the factors are as mentioned earlier in the Appendix.

For an unconcentrated single gap solar cell the maximum efficiency is limited to 31.0 %. By increasing the solar concentration to maximum the efficiency rises to 40.7% [4].

Appendix B

Detailed balance of intermediate band solar cell physics

The calculation of the efficiency for an intermediate band solar cell is a little more complicated than for the single gap solar cell. The main procedure is the same for both the recombination rate, as given in Eq (A.1), and the generation rate in Eq (A.4) [4]. However, because each of the intermediate bands has it's own flux, Φ_{ci}, Φ_{iv} and Φ_{cv} that absorb over the band gaps E_{ci}, E_{iv} and E_{cv}, respectively, see Fig. (B.1).

The generation rate for each flux must therefore be calculated and then summed up. For the recombination the integration limits must be changed. For the case where $E_{ci} < E_{iv}$ the limits become $\{E_{ci}, E_{iv}\}$, $\{E_{iv}, E_{cv}\}$ and $\{E_{cv}, \infty\}$ for the R_{ci}, R_{iv} and R_{cv} respectively.

In steady state, the sub-band gaps are to equal each other. This makes the net generation of states [4, p. 24]

$$G_{ci} - R_{ci} = G_{iv} - R_{iv} \tag{B.1}$$

As for the single junction also for the intermediate band case the electron population is described by quasi-Fermi levels. However there will be three

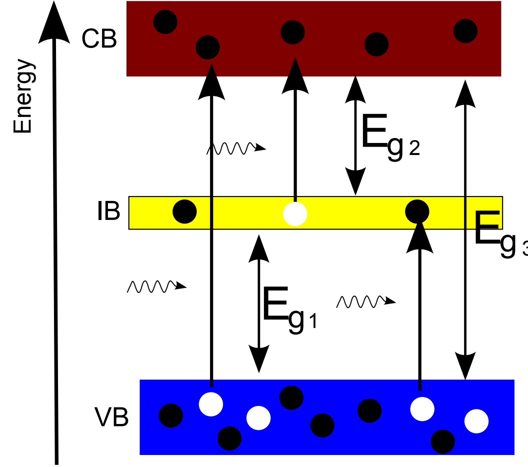

Figure B.1: *Shows the to step transition of the excitation. The excitation from the valence band to the intermediate band, labeled* E_{g1}*, from the intermediate band to the conduction band, labeled* E_{g2}*, and from the valence band to the conduction band, labeled* E_g3*.* [4, Based on Figure 3.1].

quasi-Fermi levels, $\Delta\mu_{ci}$, $\Delta\mu_{iv}$ and $\Delta\mu_{cv}$ where the two sub-band gaps equals the total quasi-Fermi level split giving

$$\Delta\mu_{cv} = \Delta\mu_{ci} + \Delta\mu_{iv} \tag{B.2}$$

By calculating the recombination rates from Eq (B.1) and Eq (B.2) the current density can be found, which is given by

$$J = q(G_{ci} - R_{ci} + G_{cv} - R_{cv}) = q(G_{iv} - R_{iv} + G_{cv} - R_{cv}) \tag{B.3}$$

For calculating the effiency of the intermediate band solar cell this J is substituted for the J in Eq (A.6). It is found that the efficiency limit is 63.2% for fully concentrated light and 46.8% for unconcentrated light. If the number of sub band gap was ∞ an efficiency at 86.8% is achievable [4].

Appendix C

Pictures of the deposition system, "The Beast"

On the next page two pictures of the deposition system used in this thesis is given. Figure (C.1) gives an overview over the system. The top, covered with grid, is the deposition chamber. In the lower area of the figure the diffusion pump is shown, colored green.The system is also coupled to water cooling and a mechanical vacuum pump which are not seen. The current is controlled with the black switch in the right of the picture.

The other picture, Fig. (C.2) shows a close-up picture of the deposition chamber. The partition is on this picture rotated $\approx 90^0$ left from the deposition up-set. The sources are attached between the prongs. The sources can be seen below the shutter. During deposition is the substrate placed on a sample holder on the top level.

Figure C.1: *An overview over the deposition system, better known as "The Beast".*

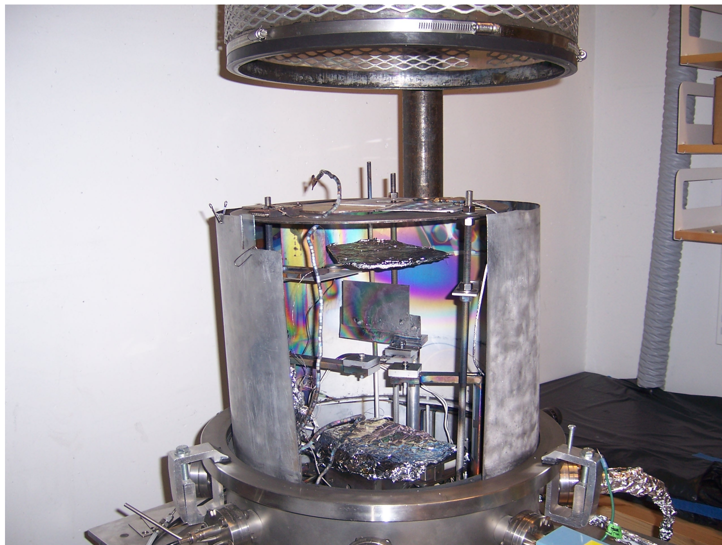

Figure C.2: *An overview inside the deposition chamber. As seen the sources are ...*

Appendix D

Datasheet, reflections of sapphire

On the next page a datasheet over possible reflections of cubic or hexagonal sapphire substrate is given. Fucluded are the 2θangle, the intensity and the repsective lattice configurations. The datasheet covers the angles from 25^0 to 153^0.

Pattern : 00-010-0173 **Radiation =** 1.540598 **Quality :** Indexed

Al_2O_3

Aluminum Oxide
Corundum, syn
Also called: alumina, alundum, diamonite

Lattice : Rhombohedral

S.G. : R-3c (167)

a = 4.75800

c = 12.99100

Z = 6

Mol. weight = 101.96

Volume [CD] = 254.70

Dx = 3.989

Dm = 4.050

I/Icor = 1.00

Optical data: A=1.7604, B=1.7686, Sign=-
Additional pattern: See ICSD 60419 (PDF 01-077-2135).
Melting point: 2050°
Additional pattern: To replace 00-043-1484.
Color: Blue, colorless, yellow purple to violet, green, pink to deep pigeon-blood red
Sample preparation: Sample annealed at 1400 C for four hours in an Al2 O3 crucible.
Analysis: Spectroscopic analysis showed <0.1% K, Na, Si; <0.01% Ca, Cu, Fe, Mg, Pb; <0.001% B, Cr, Li, Mn, Ni.
Temperature of data collection: Pattern taken at 26 C.
Common name: Also called: ruby.
Common name: Also called: sapphire.
Common name: Also called: α-Al2 O3.
Common name: Also called: α-emery.
Data collection flag: Ambient.

Natl. Bur. Stand. (U.S.), Circ. 539, volume 9, page 3 (1960)

Radiation : CuKa1

Lambda : 1.54050

SS/FOM : F30= 50(0.0188,32)

Filter : Beta

d-sp : Not given

2th	i	h	k	l
25.584	75	0	1	2
35.136	90	1	0	4
37.785	40	1	1	0
41.685	1	0	0	6
43.363	100	1	1	3
46.184	2	2	0	2
52.553	45	0	2	4
57.519	80	1	1	6
59.769	4	2	1	1
61.166	6	1	2	2
61.345	8	0	1	8
66.548	30	2	1	4
68.198	50	3	0	0
70.359	2	1	2	5
74.268	4	2	0	8
76.882	16	1	0	10
77.229	8	1	1	9
80.695	8	2	2	0
83.219	1	3	0	6
84.378	6	2	2	3
85.183	2	1	3	1
86.378	6	3	1	2
86.464	4	1	2	8
89.020	8	0	2	10
90.665	4	0	0	12
91.204	8	1	3	4
95.263	14	2	2	6
98.410	2	0	4	2
101.095	12	2	1	10
102.791	1	1	1	12
103.349	4	4	0	4
109.526	1	3	2	1
109.837	1	1	2	11
111.033	4	3	1	8
114.130	4	2	2	9
116.146	14	3	2	4
116.635	4	0	1	14
117.906	8	4	1	0
120.238	1	2	3	5
122.076	4	4	1	3
124.652	2	0	4	8
127.737	12	1	3	10
129.922	4	3	0	12
131.154	4	2	0	14
136.169	22	1	4	6
142.405	4	1	1	15
145.217	11	4	0	10
149.297	7	0	5	4
150.254	14	1	0	
152.456	13	3	3	0